Web crippling design of cold-formed stainless steel channels under interior-two-flange loading condition using deep belief network

Zhiyuan Fang[a,b], Krishanu Roy[a,*], Sujith Padiyara[b], Boshan Chen[b], Gary M. Raftery[b], James B.P. Lim[a]

[a] School of Engineering, The University of Waikato, New Zealand

[b] Department of Civil and Environmental Engineering, The University of Auckland, New Zealand

* Corresponding author: Krishanu Roy (kris.roy@waikato.ac.nz)

Abstract: This research presents a deep-learning framework, namely a deep belief network (DBN), for analyzing the interior-two-flange web crippling performance of cold-formed stainless steel channels with centered and offset web holes. An elastoplastic finite element model, validated using 101 experimental results which were previously reported in the literature, generates a total of 43,200 data points for training the DBN. When compared to a total of 54 experimental results published in the literature, the DBN predictions were shown to be approximately 10% more conservative. Using the same large training data, the developed DBN model outperformed the Backpropagation Neural Network (a typical shallow artificial neural network) and the PaddlePaddle-based linear regression model. A parametric analysis was then performed using the DBN predictions to explore the effect of section size, web holes and bearing length. Design equations for (reduced) web crippling strength are proposed for the cold-formed stainless steel perforated channels, and the feasibility of the proposed equations was assessed by the conducted reliability analysis.

Keywords: Stainless steel; Parametric study; Design equations; Deep learning; Web crippling.

1. Introduction

Cold-formed stainless steel channels are becoming increasingly popular as structural elements [1-4] due to their aesthetic appeal and good material properties, notably heat and corrosion resistance. Perforated cold-formed stainless steel channels are extensively used as bearers in floor systems because of their corrosion resistance, structural strength, and ease of installation. Web crippling is a type of localized buckling that occurs at areas of concentrated loads or excessively stressed supports in the cold-formed stainless steel channel. Current design standards specify four distinct load conditions for web crippling, including Interior-One-Flange (IOF), Interior-Two-Flange (ITF), End-One-Flange (EOF), and End-Two-Flange (ETF) loadings. This research focuses on the ITF loading condition in which both the load and support are positioned in the middle of the channel (see Fig.1). However, no comprehensive research on the web crippling behavior of such perforated cold-formed stainless steel channels under ITF loading condition is available in the literature. Besides, traditional structural analysis methods widely adopted in the design standards (i.e., ASCE 8-02 [5], AS/NZS 4673:2001 [6], and EC3 [7]) are unreliable for predicting the web crippling strength of stainless steel structures. In addition, the existing common structural analysis techniques (e.g., Finite Element Analysis (FEA)) are not efficient in producing accurate calculation results. Hence, this paper presents a deep learning (DL)-based method using a developed Deep belief neural network, which could enable quick and reliable predictions for the structural capacity of cold-formed stainless steel structures under interior-two-flange (ITF) loading (Fig.1).

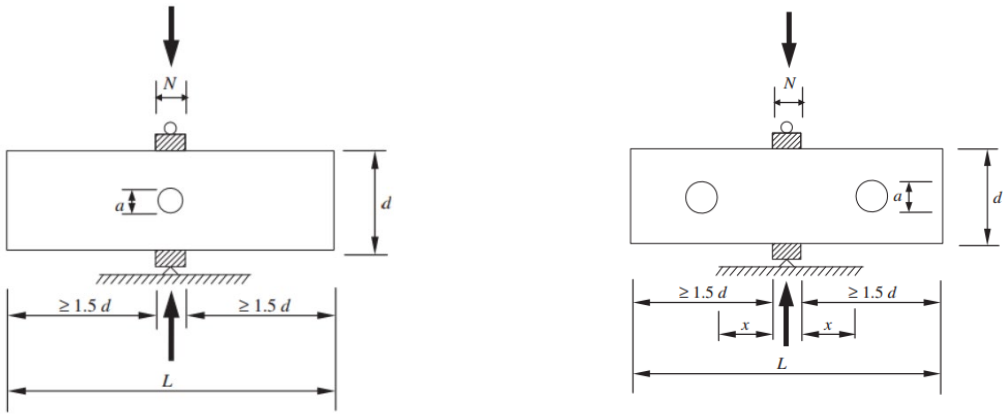

(a) Sections with center web hole under ITF loading condition

(b) Sections with offset web hole under ITF loading condition

Fig.1 Stainless steel application and ITF loading

Stainless steel is a versatile material that may be employed in structural (load-bearing) applications due to its various properties. The most prevalent stainless steel material grades are austenitic, ferritic, and duplex grades. Stainless steel has a different stress-strain relationship from carbon steel, which is virtually linear up to the yield stress point. In contrast, stainless steel has no clearly defined yield stress. The American Society of Civil Engineers Specification (ASCE 8-02) [5] shows such a relationship in Appendix C. Therefore, the newly proposed DL-based method reliably considers such a stress-strain relationship by inputting the strain hardening exponents.

Despite the ubiquity of stainless steel, few investigations on the web crippling of cold-formed stainless steel channels have been conducted. Bock et al. [8] carried out a numerical study on cold-formed stainless steel hollow and hat channel sections with ferritic cold-formed stainless steel channel sections, considering the interior-one-flange (IOF) stress condition. Santos and Gardner [9] conducted a comprehensive investigation into the structural behaviour of structural stainless steel members under concentrated traverse loading, experimentally and numerically. Four loading cases (ITF, ETF, IOF, and EOF) have been

considered in the study, and new design equations were proposed based on the experimental and FEA results. Fang et al. [10-11] investigated the structural behavior of cold-formed stainless steel channel sections with web holes under IOF and EOF loading cases, and based on the comprehensive parametric analysis, they proposed modified design equations. Yousefi et al. [12-15] recently presented experimental web crippling research on cold-formed stainless steel unlipped channel sections, although only ferritic cold-formed stainless steel was examined. Furthermore, Yousefi et al. [15] studied the web crippling behavior of lipped channels numerically and developed related design equations.

The DL- and ML- based techniques employed in this research are crucial in structural analysis for developing a strength prediction model for a challenging issue to obtain an analytic solution. Due to the good performance in exploring data features, DL has been applied to investigate the structural behavior of steel members. Liu and Zhang [16] developed an intelligent tool for quick evaluation of steel structural damage situations using a DL-based model (Convolutional Neural Network) based on the training data of over 8,000 images generated from finite element models. Ali and Cha [17] presented a DL-based approach (Deep inception neural network) for detecting concealed deterioration in steel members based on a total of 2,000 thermal images. Using a total of 5,000 training data from Finite element analysis (FEA), Hung et al. [18] used Deep Neural Network to estimate the ultimate load-carrying capability of steel trusses. Papazafeiropoulos et al. [19] employed Deep Neural Network to investigate the buckling behavior of strengthened steel plate girders using a total of 2,200 training data. Xu et al. [20] investigated the bearing capacity of stainless steel circular hollow section columns using Random Forest and XGBoost tools based on a total of

280 test data collected from the literature. Fang et al. [21] applied the eXtreme Gradient Boosting (XGBoost) tool to investigate the structural behaviour of roll-formed aluminium alloy beams using over 1,000 data points generated from FEA. Similarly, Dai et al. [22] used the XGBoost tool to investigate the moment capacity of cold-formed steel beams based on a total of 1,620 data points generated from FEA. Fang et al. [23-27] used a developed Deep Belief Network (DBN) to conduct the structural analysis of thin-walled structures under different loading conditions based on thousands of data points generated from FEA. It should be noted that Fang et al. [23] investigated the ETF web crippling behavior of cold-formed stainless steel channels, and the similar methods were adopted in the current study to explore the ITF web crippling behavior of cold-formed stainless steel channels.

The purpose of this research is to present a novel DBN framework for investigating the ITF structural behavior of cold-formed stainless steel perforated channels. The three most common stainless steel grades were used in this investigation: S43000 ferritic stainless steel, S32205 duplex stainless steel, and S30400 austenitic stainless steel. A validated elastoplastic finite element model was used to generate 43,200 data points for training the DBN. The absolute percentage error was used to evaluate the prediction performance of various approaches, including the developed DBN model, the Backpropagation Neural Network (a typical shallow artificial neural network) and the PaddlePaddle-based linear regression model [28]. After its accuracy was demonstrated with regards to the prediction of the web crippling strength, the developed DBN was used to investigate the effect of section size, web hole and bearing length of the structural behavior of cold-formed stainless steel perforated channels subjected to ITF loading. The design equations for ITF web crippling strength for cold-

formed stainless steel perforated channels were proposed, and the feasibility of such equations was assessed through a reliability analysis.

2 Numerical simulation

2.1 General

ABAQUS [29] was used to develop a FE model for cold-formed stainless steel channels under ITF loading condition (Fig.2(a)). S4R shell elements were used to model the cold-formed stainless steel channels. The mesh sizes of 5mm × 5mm and 10mm × 10mm were suitable for modelling the cold-formed stainless steel channels and bearing plate, respectively. Mesh refinement (See Fig.2(b)) was performed around rounded corner and web holes to achieve highly accurate results from the FEA.

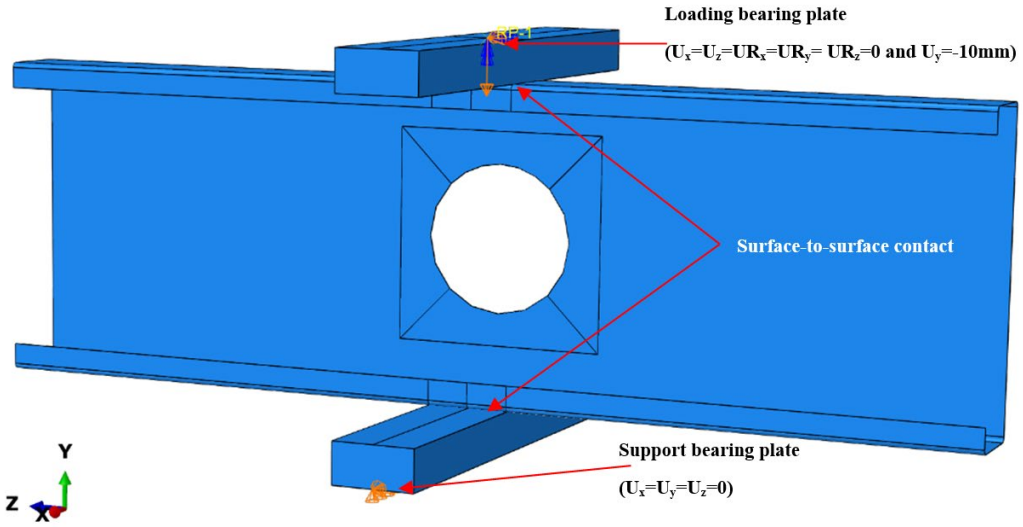

(a) FE boundary setting

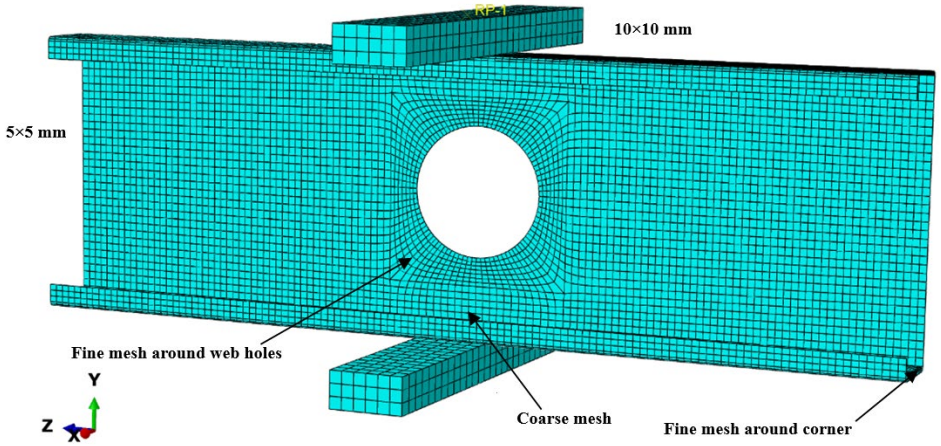

(b) FE meshing

Fig.2 FE modelling

2.2 Material property

The material properties of S43000 ferritic stainless steel, S32205 duplex stainless steel, and S30400 austenitic stainless steel were used in the FE modeling. It is noted that the corner enhancement due to the cold-forming procedure will bring about higher strength material properties in the corner part of the sections, however, the enhanced effect of the corner part on the web crippling is negligible in the current study, which has already been confirmed by Yousefi et al. [12-17]. Table 1 shows the mechanical properties. According to Arrayago et al. [30], Mirambell and Real [31], and Rasmussen [32], the material stress-strain relationship follows equation 1 as shown below:

$$\varepsilon=\begin{cases} \dfrac{f}{E}+0.002\left(\dfrac{f}{f_{0.2}}\right)^{n} & f \le f_y \\ \dfrac{f-f_{0.2}}{E_{0.2}}+\left(\varepsilon_u-\varepsilon_{0.2}-\dfrac{f_u-f_{0.2}}{E_{0.2}}\right)\left(\dfrac{f-f_{0.2}}{f_u-f_{0.2}}\right)^{m}+\varepsilon_{0.2} & f_y \prec f \le f_u \end{cases} \quad (1)$$

Where,

$$E_{0.2}=\frac{E}{1+0.002n\dfrac{E}{f_{0.2}}} \quad (2)$$

For ferritic stainless steel, $\varepsilon_u=0.6\left(1-\dfrac{f_{0.2}}{f_u}\right)$ (3)

For duplex and austenitic stainless steel, $\varepsilon_u=1-\dfrac{f_{0.2}}{f_u}$ (4)

Where, E and $E_{0.2}$ are the Young's modulus and tangent modulus at 0.2% of proof stress, respectively; $f_{0.2}$ is 0.2% of proof stress; m and n are the strain hardening exponents; f_y, f_u and ε_u are yield stress, ultimate stress and ultimate strain, respectively.

Table 1 Stainless steel material properties

Steel grade / Index	S43000 ferritic		S32205 duplex	S30400 austenitic
Yield stress (MPa)	205	284	450	205
Ultimate stress (MPa)	450	462	655	515
m	2.5	3.03	3.27	2.31
n	14	14	8	7

2.3 Loading procedure and boundary conditions

The surface-to-surface contact setting was implemented to simulate the interaction between the bearing plate and the channel portion (see Fig.2(a)). The target surface was chosen as the bearing plate and the channel was selected as the contact surface. The 'hard' contact property setting was applied to prevent penetration of the two contact surfaces.

Displacement control was used to simulate vertical force applied to the channels. The nodes of the top bearing plate where the vertical load was applied were subjected to an induced displacement. The top bearing plate was restricted for movement in all degrees of freedom with exception of translational degree of freedom in the vertical direction.

2.4 Validation of FE model

2.4.1 Corner meshing on FE model performance

Mesh convergence entails reducing the element size and analysing the effect of this reduction on the solution's precision. Typically, the smaller the mesh size, the more accurate the solution, as the behaviour of the structural member is sampled more thoroughly over its physical domain. Nevertheless, the greater the accuracy, the greater the simulations might get in terms of data to store and manage, which results in longer simulation runtimes. Besides, from the previous studies [12-13], it is known that the corner mesh size will affect the numerical simulation accuracy significantly. Therefore, in the present study, we conducted a

mesh convergence analysis mainly to determine the ideal corner mesh size in terms of accuracy and computational time. Table 2 and Fig. 3 show the results of the corner meshing analysis undertaken in this study for specimens (ID:38-43 from Table 3(b)). The ratio of experimental strength (P_{EXP}) to FEA strength (P_{FEA}) declines from 1.074 to 1.050 when the mesh number per radius around the corner increases from 0.6 to 3.4. When the mesh number per radius is bigger than 6, the average ratio (P_{EXP}/P_{FEA}) remains almost constant at 1.05. Therefore, in order to optimize computational time and to improve the accuracy of the FE predictions, the mesh number per radius around the corner was set at 1.2 in the FE models. Similar mesh convergence study methods have been employed by Dar et al. [33] and Zhang et al. [34].

Table 2 Mesh sensitivity analysis of selected specimens from the literature [35-37]

Mesh number per radius around corner	Average number of elements in total	Average P_{EXP}/P_{FEA}
3.4	17906	1.050
2.2	14842	1.051
1.4	12800	1.051
1.2	12289	1.052
0.8	11268	1.071
0.6	10757	1.074

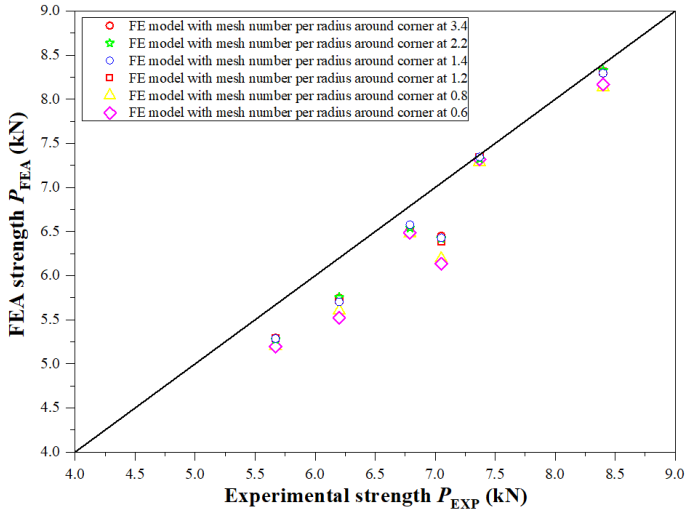

Fig.3 Experimental strength and FEA strength of specimens (ID=38-43) at varied mesh size around the corner regions of CFS channels

158 *2.4.2 FE validation*

159 The FE validation was based on Yousefi et al. [12-13] and Uzzaman et al. [35-37] (see

160 Table 3 and Fig.4). Table 3 and Fig.4 show that for unfastened sections and fastened sections,

161 the ratios of F_{EXP}/F_{FEA} are 1.01 and 0.97, respectively.

Table 3 FE validation

(a) Unfastened sections

Specimen ID	Web	Flange	Lip	Bend radius	Thickness	Hole dia	Bearing length	Yield stress	Exp.load	FEA result	P_{EXP}/P_{FEA}
	d/mm	b_f/mm	b_l/mm	R/mm	t/mm	a/mm	N/mm	f_y/MPa	P_{EXP}/kN	P_{FEA}/kN	
1	178.63	60.13	0	1.2	1.13	0	50	284	4.16	4.16	1.00
2	178.12	60.27	0	1.2	1.14	69	50	284	3.71	3.70	1.00
3	178.55	59.98	0	1.2	1.12	68.89	50	284	3.29	3.38	0.97
4	178.56	60.04	0	1.2	1.12	0	75	284	4.28	4.20	1.02
5	178.66	60.05	0	1.2	1.10	68.74	75	284	3.66	3.50	1.05
6	178.44	60.09	0	1.2	1.12	68.8	75	284	3.34	3.56	0.94
7	178.49	60.1	0	1.2	1.12	0	100	284	4.52	4.34	1.04
8	178.46	60.11	0	1.2	1.11	68.87	100	284	3.84	3.71	1.03
9	178.55	60.09	0	1.2	1.09	68.7	100	284	3.41	3.46	0.98
10	203.86	74.99	0	1.2	1.09	0	50	284	3.40	3.43	0.99
11	203.62	75.01	0	1.2	1.08	78.92	50	284	3.03	2.96	1.02
12	203.69	74.92	0	1.2	1.10	78.7	50	284	2.85	2.94	0.97
13	203.44	75.02	0	1.2	1.08	0	75	284	3.49	3.47	1.00
14	203.53	75.06	0	1.2	1.06	78.9	75	284	3.06	2.92	1.05
15	203.42	75.11	0	1.2	1.06	78.9	75	284	2.77	2.77	1.00
16	203.64	74.99	0	1.2	1.12	0	100	284	4.16	3.96	1.05
17	203.73	75.02	0	1.2	1.09	78.93	100	284	3.47	3.25	1.07
18	203.77	74.84	0	1.2	1.06	78.9	100	284	2.86	2.88	0.99
19	253.55	100.16	0	1.2	1.02	0	50	284	2.44	2.36	1.04
20	253.53	100.78	0	1.2	1.04	98.81	50	284	2.20	2.24	0.98
21	253.75	99.73	0	1.2	1.00	98.87	50	284	1.91	1.88	1.02
22	255.03	100.15	0	1.2	1.07	0	75	284	2.99	2.76	1.08
23	254.03	100.24	0	1.2	1.10	98.82	75	284	2.70	2.70	1.00
24	253.32	102.47	0	1.2	1.08	98.86	75	284	2.51	2.44	1.03
25	253.5	99.93	0	1.2	1.11	0	100	284	3.39	3.19	1.06
26	253.45	100.04	0	1.2	1.08	98.86	100	284	2.82	2.65	1.06
27	253.41	99.91	0	1.2	1.09	98.84	100	284	2.59	2.59	1.00
Average											1.02
Cov											0.03
28	142.2	58.6	15.9	4.8	1.23	0	90	455	6.03	5.73	1.05
29	142.2	58.6	15.9	4.8	1.23	27.9	90	455	5.96	5.54	1.08
30	142.2	59.5	16.3	4.8	1.25	55.8	90	455	5.45	5.34	1.02
31	142.2	59.5	16.3	4.8	1.25	83.6	90	455	4.52	4.73	0.96
32	142.2	59.5	16.3	4.8	1.25	111.5	90	455	3.52	3.80	0.93
33	141.8	58.9	15.6	4.8	1.24	0	120	455	6.32	6.18	1.02
34	141.8	58.9	15.6	4.8	1.24	27.9	120	455	6.05	5.96	1.01
35	141.3	58.8	16.3	4.8	1.24	55.7	120	455	5.45	5.54	0.98
36	141.3	58.8	16.3	4.8	1.24	83.6	120	455	4.75	4.96	0.96
37	142.2	59.5	16.3	4.8	1.25	111.5	120	455	3.79	4.17	0.91
38	172.8	64.1	15.6	5	1.27	0	120	534	7.05	6.39	1.10

39	172.3	63.6	15.5	5	1.27	67.6	120	534	6.20	5.73	1.08
40	172.6	64.3	15.3	5	1.28	101.6	120	534	5.67	5.29	1.07
41	202.1	63.1	17.5	5	1.45	0	150	513	8.40	8.31	1.01
42	202.7	64.3	16.3	5	1.45	79.5	150	513	7.37	7.34	1.00
43	202.4	64.2	16.5	5	1.45	119.5	150	513	6.79	6.52	1.04
44	263.4	63.4	14.4	5.5	1.56	0	150	525	8.19	7.80	1.05
45	262.8	63.4	14.7	5.5	1.55	51.8	150	525	7.88	7.39	1.07
46	262.8	63.4	14.7	5.5	1.55	103.5	150	525	7.29	6.83	1.07
Average											1.02
Cov											0.05
47	290.33	45.51	18.01	3	2.46	0	50	265.7	22.13	21.51	1.03
48	289.33	45.37	18.55	3	2.47	0	75	265.7	22.65	22.23	1.02
49	290.67	45.35	18.47	3	2.47	0	100	265.7	23.11	22.49	1.03
50	290	45.31	18.22	3	2.48	140	50	326.8	15.10	15.84	0.95
51	289	45.27	18.24	3	2.48	140	75	326.8	15.60	16.31	0.96
52	290	44.6	19.57	3	2.48	140	100	326.8	16.11	16.73	0.96
53	289	44.59	20.33	3	2.48	140	50	326.8	15.77	16.95	0.93
54	289	44.62	20.24	3	2.47	140	75	326.8	16.72	17.17	0.97
55	289	44.6	20.23	3	2.47	140	100	326.8	17.02	17.55	0.97
Average											0.98
Cov											0.03

(b) Fastened sections

Specimen ID	Web	Flange	Lip	Bend radius	Thickness	Hole dia	Bearing length	Yield stress	Exp.load	FEA result	P_{EXP}/P_{FEA}
	d/mm	b_f/mm	b_l/mm	R/mm	t/mm	a/mm	N/mm	f_y/MPa	P_{EXP}/kN	P_{FEA}/kN	
1	178.4	60.17	0	1.2	1.13	0	50	284	6.68	6.51	1.03
2	178.51	60.08	0	1.2	1.13	68.86	50	284	5.68	5.44	1.04
3	178.43	60.02	0	1.2	1.08	68.85	50	284	5.44	4.92	1.11
4	178.3	60.09	0	1.2	1.14	0	75	284	6.66	6.63	1.00
5	178.38	60.09	0	1.2	1.12	68.7	75	284	5.37	5.51	0.98
6	178.42	60	0	1.2	1.08	68.87	75	284	5.60	5.05	1.11
7	178.43	59.99	0	1.2	1.14	0	100	284	6.78	6.81	1.00
8	178.66	60.03	0	1.2	1.12	68.84	100	284	5.65	5.67	1.00
9	178.4	60.15	0	1.2	1.10	68.81	100	284	5.37	5.23	1.03
10	203.68	75.05	0	1.2	1.13	0	50	284	5.82	6.32	0.92
11	203.68	75.13	0	1.2	1.10	78.95	50	284	4.90	5.11	0.96
12	203.46	75.14	0	1.2	1.07	78.87	50	284	4.99	4.67	1.07
13	203.63	75.49	0	1.2	1.14	0	75	284	5.82	6.53	0.89
14	203.78	75.04	0	1.2	1.13	78.92	75	284	4.81	5.42	0.89
15	203.48	75.12	0	1.2	1.08	78.85	75	284	4.67	4.91	0.95
16	203.61	75.21	0	1.2	1.14	0	100	284	6.50	6.61	0.98
17	203.47	75.04	0	1.2	1.12	78.9	100	284	5.27	5.52	0.96
18	203.54	75.37	0	1.2	1.09	78.87	100	284	4.78	5.10	0.94
19	254.17	99.89	0	1.2	1.14	0	50	284	4.33	5.83	0.74
20	253.88	99.99	0	1.2	1.10	98.9	50	284	4.07	4.72	0.86
21	253.87	99.94	0	1.2	1.09	98.87	50	284	3.45	4.41	0.78
22	253.87	99.98	0	1.2	1.14	0	75	284	4.98	5.95	0.84
23	253.86	100.05	0	1.2	1.09	98.88	75	284	4.79	4.86	0.99
24	253.75	99.86	0	1.2	1.07	98.82	75	284	4.39	4.36	1.01
25	253.55	99.92	0	1.2	1.14	0	100	284	5.65	6.09	0.93
26	253.61	100	0	1.2	1.12	98.83	100	284	4.68	4.97	0.94
27	253.14	100.02	0	1.2	1.09	98.84	100	284	4.56	4.64	0.98
Average											0.96
Cov											0.09
28	142.2	58.6	15.9	4.8	1.23	0	90	455	8.97	9.27	0.97

29	142.2	58.6	15.9	4.8	1.23	27.9	90	455	8.96	8.94	1.00
30	142.2	59.5	16.3	4.8	1.25	55.8	90	455	7.75	8.39	0.92
31	142.2	59.5	16.3	4.8	1.25	83.6	90	455	6.64	7.08	0.94
32	142.2	59.5	16.3	4.8	1.25	111.5	90	455	5.55	5.87	0.95
33	141.8	58.9	15.6	4.8	1.24	0	120	455	9.44	9.89	0.95
34	141.8	58.9	15.6	4.8	1.24	27.9	120	455	9.26	9.55	0.97
35	141.3	58.8	16.3	4.8	1.24	55.7	120	455	8.19	8.70	0.94
36	141.3	58.8	16.3	4.8	1.24	83.6	120	455	7.06	7.49	0.94
37	142.2	59.5	16.3	4.8	1.25	111.5	120	455	5.94	6.41	0.93
38	172.8	64.1	15.6	5	1.27	0	120	534	10.72	10.21	1.05
39	172.3	63.6	15.5	5	1.27	67.6	120	534	9.31	9.11	1.02
40	172.6	64.3	15.3	5	1.28	101.6	120	534	7.87	7.87	1.00
41	202.1	63.1	17.5	5	1.45	0	150	513	13.51	12.84	1.05
42	202.7	64.3	16.3	5	1.45	79.5	150	513	11.42	11.48	0.99
43	202.4	64.2	16.5	5	1.45	119.5	150	513	10.10	9.91	1.02
44	263.4	63.4	14.4	5.5	1.56	0	150	525	12.78	12.52	1.02
45	262.8	63.4	14.7	5.5	1.55	51.8	150	525	12.41	11.99	1.03
46	262.8	63.4	14.7	5.5	1.55	103.5	150	525	11.31	11.18	1.01
Average											0.99
Cov											0.04

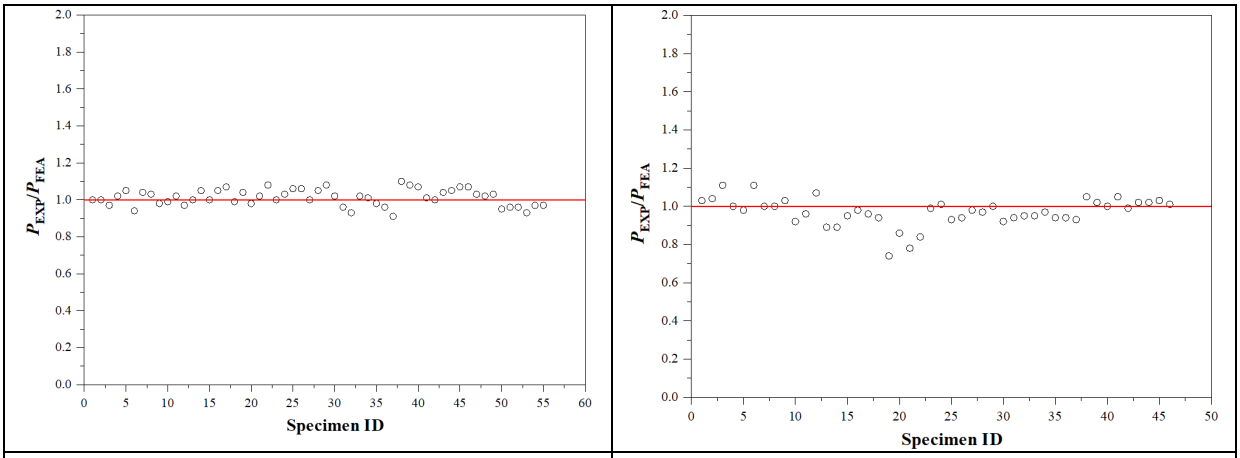

(a) Unfastened sections (b) Fastened sections

Fig.4 FE validation

3 Design guidelines

3.1 Web crippling strength

3.1.1 ASCE 8-02 [5]

For cold-formed stainless steel channels, ITF web crippling strength (P_{ASCE}) can be determined by the equations (5) of ASCE 8-02 [5]:

$$P_{ASCE} = t^2 C_1 C_2 C_\theta C_t (771 - 2.26\frac{h}{t})(1 + 0.0013\frac{N}{t}) \quad (5)$$

Where, C_1, C_2, C_θ, C_l are coefficients taken from ASCE 8-02 [5].

3.1.2 AISI&AS/NZS [38-39]

The AISI&AS/NZS [38-39] provide unified web crippling design formulae for CFCS sections with varying coefficients:

$$P_{AISI\&AS/NZS} = Ct^2 f_y \sin\theta(1-C_w\sqrt{\frac{h}{t}})(1-C_r\sqrt{\frac{r}{t}})(1+C_l\sqrt{\frac{N}{t}}) \quad (6)$$

where N is the bearing length; C, C_r, C_l and C_w are the coefficients obtained from AISI&AS/NZS [38-39].

3.1.3 Eurocode 3 [40]

Eurocode 3 (EC3) [40] offers design formulae for ITF web crippling strength of CFCS channels:

$$P_{EC} = k_3 k_4 k_5[21.0-\frac{d_w/t}{16.3}][1+0.0013\frac{N}{t}]t^2 f_y \quad (13)$$

Where, k_3, k_4, k_5 are coefficients taken from EC3 [40]; d_w is the web height.

3.2 Web crippling strength reduction factor

Yousefi et al. [12-13] proposed ITF web crippling strength reduction factor equations for ferritic channels; however, the investigated sections are all unlipped. Therefore, the proposed design equations could be used for the ferritic, duplex, and austenitic channels in this study. Compared to the previous study [12-13], the limits of such equations are enlarged to $h/t \leq 157.68$, $N/t \leq 120.97$, $N/h \leq 1.15$, and $a/h \leq 0.8$. However, unlike the previous study [12-13], the effect of the bearing length on the reduction factor is included in the proposed equations.

4 Deep Belief Network (DBN)

4.1 General

DBN is a deep network consisting of many Restricted Boltzmann Machine (RBM) [41] layers and one Backpropagation Neural Network layer. DBN combines unsupervised pretraining with supervised fine-tuning. DBN converts low-level features to high-level and abstract representation attribute categories or features to investigate distributed data feature representation [42]. DBN optimizes the initial values of network parameters throughout the training process, potentially avoiding the trap of local optimum values caused by random startup settings. Using several hidden layers with multiply-units can aid in obtaining more meaningful data features. However, direct training of a multiple-layer network may result in mis-convergence. Unsupervised layer-wise pretraining is employed in the DBN training process to avoid mis-convergence induced as a result of model complexity.

Normalization was applied to both the input and output layers. For every 50 epochs in each run, the cross-validation error was evaluated, and the training was stopped when the error did not improve or when the 20,000 epochs limit was reached. The best run (according to the cross-validation criterion) was chosen from each set of 20 runs, and the following statistical characteristics were tested:

$$\mathrm{Err}_i(\%) = \frac{|y_i - t_i|}{t_i} \times 100 \tag{14}$$

$$R^* = \frac{\sum_{i=1}^{n_d} (y_i - \overline{y_i})(t_i - \overline{t_i})}{\sqrt{\sum_{i=1}^{n_d} (y_i - \overline{y_i})^2 \sum_{i=1}^{n_d} (t_i - \overline{t_i})^2}} \tag{15}$$

$$\mathrm{MSE} = \frac{1}{n_d} \sum_{i=1}^{n_d} (t_i - y_i)^2 \tag{16}$$

$$\mathrm{MAE} = \frac{1}{n_d}\sum_{i=1}^{n_d}\left|y_i - t_i\right| \tag{17}$$

Where, t_i and y_i represent the actual and prediction output values for the i^{th} output, respectively. $\overline{t_i}$ and $\overline{y_i}$ are the mean values of actual and predicted outputs, respectively, and n_d denotes the number of data series. Err, R*, MSE, MAE are absolute percentage error, correlation coefficient, mean squared error and mean absolute error, respectively.

4.2 Restricted Boltzmann machine

Restricted Boltzmann machine is a stochastic neural network capable of learning a distribution across its input set. The network typically consists of one layer of visible neurons with binary values and one layer of hidden units with Boolean values. In an RBM, no connections occur between neurons in the same layer, while complete connections exist between neurons in separate levels. Meanwhile, these links are bidirectional and symmetrical.

RBM is capable of learning a probability distribution from the visible layer to the hidden layer, allowing its setup to display desired attributes. The learning process is carried out by the use of an energy function. Given the visible units v_i, the hidden units h_j, and their connection weights W_{ij} (size $n_v \times n_h$), together with the offset ai for v_i and the bias weight b_j for h_j, the energy function E(v, h) of a certain configuration can be constructed as follows.

$$E(v,h) = -\sum_{i=1}^{n_v} a_i v_i - \sum_{j=1}^{n_h} b_j h_j - \sum_{i=1}^{n_v}\sum_{j=1}^{n_h} h_j w_{j,i} v_i \tag{18}$$

The joint probability distribution for the visible and hidden vectors is defined as follows in terms of the energy function:

$$P(v,h) = \frac{1}{Z}e^{-E(v,h)} \tag{19}$$

$$Z = \sum_{v}\sum_{h} e^{-E(v,h)} \tag{20}$$

Where Z is a partition function.

The conditional probability of a configuration of visible units v_i, given h, or of h_j given v is provided for n_v visible units and n_h hidden units:

$$P(v|h) = \prod_{i=1}^{n_v} P(v_i|h) \tag{21}$$

$$P(h|v) = \prod_{j=1}^{n_h} P(h_j|v) \tag{22}$$

4.3 Extraction of data feature

The Denoising Auto Encoder (DAE) is an unsupervised neural network that trains on unlabeled input. Even though the features are learned without the inclusion of label information, the data features formed by DAE learning retain the bulk of the information from the input data. For supervised learning tasks such as regression predictions based on small amounts of data, there is a considerable relationship between feature extraction and label information. Therefore, adding label information to the DAE output layer can increase the applicability of the model's features for regression prediction. Fig.5(a) depicts the DAE training process. The training process of DAE was followed by performing the steps given below: Step 1: Adding noise and assuming that the noise percentage of the developed DAE is k, noise was added in line with the noise percentage k to the input layer sample. x^* was the new input sample; Step 2: Compute the feature of hidden layer $h = \{h_1, h_2, \ldots, h_m\}$;Compute the value of output layer y'; Step 3: Compute the loss function $L(y, y')$ and its derivatives, update the parameters until convergence, according to reverse direction of gradient. The Stacked Denoising Auto Encoder (SDAE) was a string of DAEs that was used to extract the data features in this study. Fig.5(b) depicts the structure of SDAE.

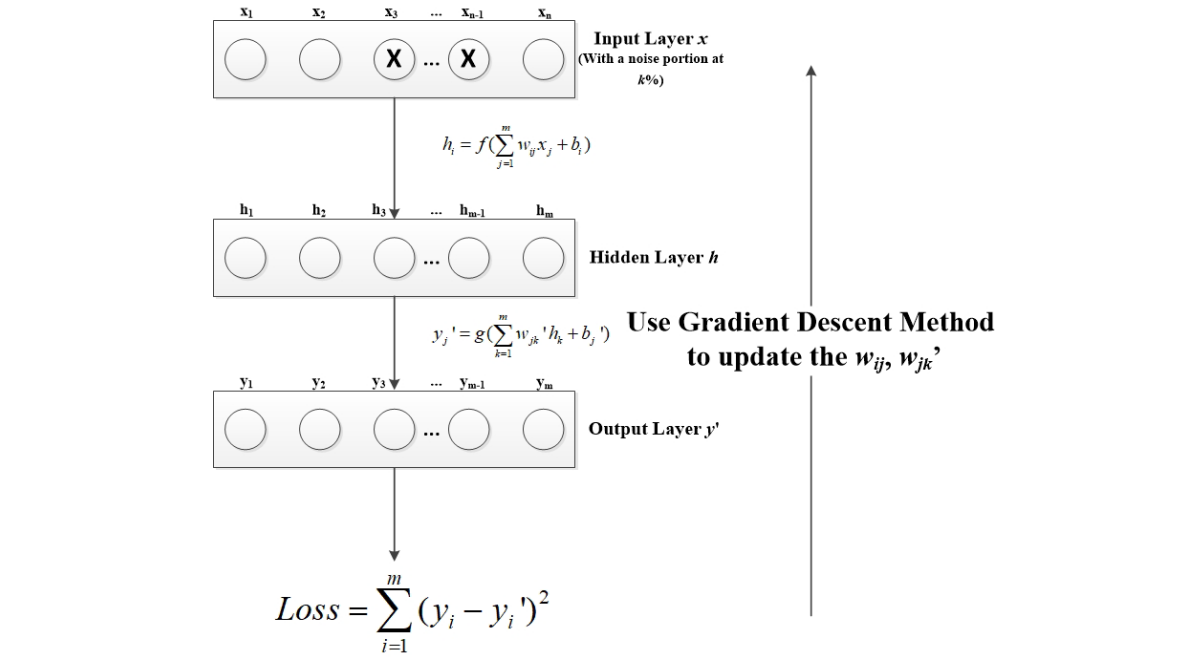

(a) DAE training

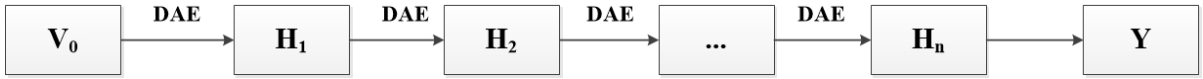

(b) SDAE structures

Fig.5 Data feature extraction method [23-27]

251

252 *4.4 Optimization of hyperparameter*

253 The hyperparameters were optimized using the Block Changing Grid Search (BCGS)
254 method. The Block Grid Search was used to build the BCGS. The Local Support Vector
255 Machine (LSVM) [43] was used to determine the strength. The hyperparameters were the
256 number of hidden layers, the block size of BCGS, and the learning rate. In training, the
257 number of hidden layers does not exceed 500. Regarding other hyperparameters, there are no
258 limitations. Hence, the steps outlined below were used to carry out the BCGS procedure: First,
259 all hyperparameters are organised into groups, and each has two distinct value ranges;
260 Secondly, the BGS algorithm was then executed using the initial set of values. Thirdly, the
261 hyper-parameters were updated using the second set of values, and the BGS technique was
262 used to optimize the grid; The last step is to repeat steps 2 and 3 until the ideal combination
263 of the generated hyper-parameters remains constant.

264 *4.5 Data training*

265 A total of 43,200 numerical data points generated by validated FE models were
266 randomly divided into three groups. 50% of the data points are utilised for training, 25% for
267 validation, and the rest for testing. To create the database of training data, the following
268 parameters were randomly varied: depth of the web (b_w) from 100 mm to 300 mm; thickness
269 of the channel (t) from 0.5 mm to 2.5 mm; length of the CFS channel sections (L) from 380
270 mm to 1000 mm; ratio of the hole diameter to web height (a/h) from 0 to 0.8. The FEA
271 results of the database were varied from 0.3 to 45 kN. The neural network's input and output
272 are as follows:

273 $$\text{Input} = \left\{ b_w, b_l, b_f, t, N, a, x, f_y, m, n \right\} \tag{23}$$

$$\text{Output} = \{P_c\} \tag{24}$$

Where, b_w, b_f, b_l, t and N are the web depth, flange length, lip length, section thickness and bearing length. a is the diameter to the web hole. x represents the distance of the hole to the bearing block. P_c and P_p are the actual and predicted web crippling strengths, respectively. m and n are the strain hardening exponents of the stainless steel.

To speed up the learning process and to obtain accurate results, input and output data series were normalized using the following formula:

$$X_{si} = \frac{(X_i - \overline{X})}{(X_{\max} - X_{\min})} \tag{25}$$

where X_i is the value of i^{th} variable, and $\overline{X}$ is the mean value of variables.

The early stopping technique to facilitate data processing was employed to minimize over-fitting situations. During the data analysis, specific data sets with poor performance were removed. After multiple trial-and-error simulations, the number of neurons in DBN's hidden layer was determined. For 43,200 FEA data points, the training time for convergence was less than 60 minutes. The input and output data series were normalized to ensure reliable outcomes. The DBN training process is shown in Fig.6.

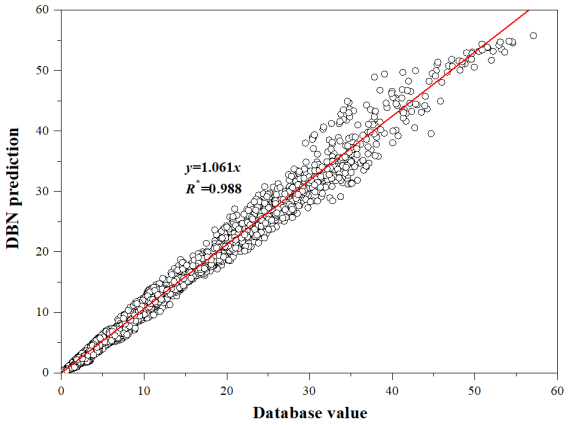

(a) Training set

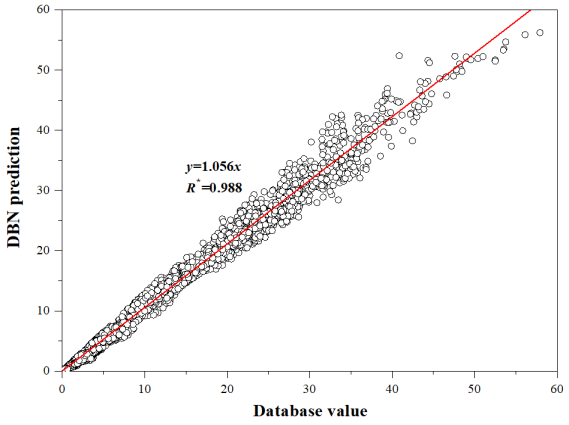

(b) Validation set

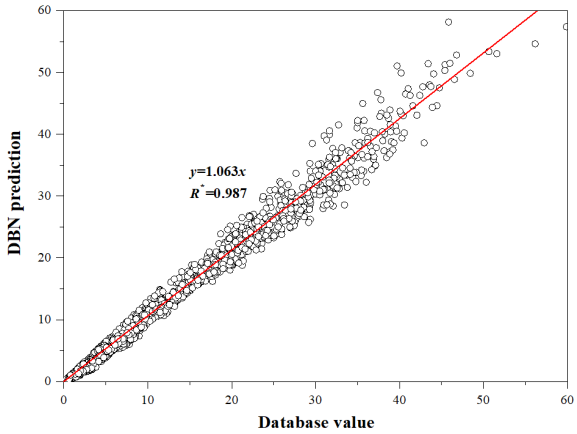

(c) Testing set

Fig.6 DBN training

5 Assessment of DBN prediction

Table 4 summarizes and details the prediction performance of the DBN, BPN, and Paddle models. The parameters (R*, MSE, and MAE) are utilized to assess each model's prediction performance, as shown in Table 5. The average Err for unfastened sections based on FEA data, as well as design strengths from ASCE 8-02 [5], EC3 [40], and AISI&AS/NZS [38-39], and results obtained from the DBN, BPN, and Paddle models, are 2.9 %, 9.8 %, 14.0 %, 15.0 %, 6.8 %, 24.9% and 19.2 %, respectively, in Fig.7 and Table 4. Similarly, 7.0 %, 36.5 %, 43.7 %, 3.8%, 4.9 %, 11.4 %, and 10.3 % are the values for fastened sections. It can be concluded from Fig.7 and Table 4 that both the FEA and DBN results are more accurate in determining the web crippling strength of cold-formed stainless steel perforated channels.

Table 4 Absolute percentage error from various methods

(a) Unfastened sections

Specimen ID	Web	Flange	Thickness	Experimental load	Err/%						
	d	b_f	t	P_{EXP}	FEA	ASCE	EC	AISI&AS/NZS	DBN	BPN	Paddle
	(mm)	(mm)	(mm)	(kN)							
1	178.63	60.13	1.13	4.16	0.1	10.75	1.44	21.87	10.67	33.36	33.98
2-center hole	178.12	60.27	1.14	3.71	0.32	--	--	--	11.09	25.06	13.72
3-offset hole	178.55	59.98	1.12	3.29	2.88	--	--	--	11.24	30.61	20.17
4	178.56	60.04	1.12	4.28	1.88	7.86	1.4	15.39	10.92	19.34	11.63
5-center hole	178.66	60.05	1.1	3.66	4.47	--	--	--	12.86	37.06	34.6
6-offset hole	178.44	60.09	1.12	3.34	6.65	--	--	--	7.48	16.3	10.21
7	178.49	60.1	1.12	4.52	3.9	4.89	3.98	11.54	12.37	32.68	15
8-center hole	178.46	60.11	1.11	3.84	3.28	--	--	--	11.34	24.65	27.99
9-offset hole	178.55	60.09	1.09	3.41	1.54	--	--	--	11.03	32.77	14.97
10	203.86	74.99	1.09	3.4	0.96	6.49	12.35	19.4	3.98	12.29	26.55
11-center hole	203.62	75.01	1.08	3.03	2.22	--	--	--	8.63	39.92	14.94
12-offset hole	203.69	74.92	1.1	2.85	3.19	--	--	--	6.05	39.98	19.05
13	203.44	75.02	1.08	3.49	0.43	3.85	14.61	12.52	4.03	15.67	19.18
14-center hole	203.53	75.06	1.06	3.06	4.54	--	--	--	8.95	15.04	39.52
15-offset hole	203.42	75.11	1.06	2.77	0.08	--	--	--	6.84	42.7	19.88
16	203.64	74.99	1.12	4.16	4.84	0.13	17.31	10.56	8.54	15.26	12.84
17-center hole	203.73	75.02	1.09	3.47	6.26	--	--	--	10.18	33.13	22.6
18-offset hole	203.77	74.84	1.06	2.86	0.86	--	--	--	5.51	7.33	9.05
19	253.55	100.16	1.02	2.44	3.46	20.83	27.87	20.7	4.23	11.98	22.58
20-center hole	253.53	100.78	1.04	2.2	1.85	--	--	--	5.18	39.34	6.79
21-offset hole	253.75	99.73	1	1.91	1.79	--	--	--	0.9	35.54	34.29
22	255.03	100.15	1.07	2.99	7.68	19.11	26.09	15.08	0.72	26.88	20.59
23-center hole	254.03	100.24	1.1	2.7	0.16	--	--	--	4.14	31.37	26.37
24-offset hole	253.32	102.47	1.08	2.51	2.88	--	--	--	1.13	28.35	1.57
25	253.5	99.93	1.11	3.39	5.9	13.85	21.24	7.5	1.56	13.07	10.52
26-center hole	253.45	100.04	1.08	2.82	5.94	--	--	--	0.67	7.11	3.92
27-offset hole	253.41	99.91	1.09	2.59	0.15	--	--	--	2.57	5.16	25.23
Average					2.9	9.75	14.03	14.95	6.77	24.89	19.17
Cov					2.23	6.61	9.55	4.63	3.95	11.31	9.59

(b) Fastened sections

Specimen ID	Web	Flange	Thickness	Experimental load	Err/%						
	d	b_f	t	P_{EXP}	FEA	ASCE	EC	AISI&AS/NZS	DBN	BPN	Paddle
	(mm)	(mm)	(mm)	(kN)							
1	178.4	60.17	1.13	6.51	2.48	29.15	35.18	5.94	11.61	25.66	23.01
2-center hole	178.51	60.08	1.13	5.44	4.23				8.31	10.83	17.62
3-offset hole	178.43	60.02	1.08	4.92	9.61				9.55	20.22	26.78
4	178.3	60.09	1.14	6.63	0.4	26.72	32.88	1.51	5.74	20.5	8.14
5-center hole	178.38	60.09	1.12	5.51	2.56				5.03	13.28	11.19
6-offset hole	178.42	60	1.08	5.05	9.86				6.52	13.53	16.48
7	178.43	59.99	1.14	6.81	0.41	26.83	33.04	4.82	3.44	11.74	14.5
8-center hole	178.66	60.03	1.12	5.67	0.29				2.7	12.44	11.15
9-offset hole	178.4	60.15	1.1	5.23	2.69				1.82	4.84	4.52
10	203.68	75.05	1.13	6.32	8.53	35.78	46.84	7.36	9.03	17.11	9.47
11-center hole	203.68	75.13	1.1	5.11	4.18				7.89	19.19	11.27
12-offset hole	203.46	75.14	1.07	4.67	6.5				6.57	14.54	8.67
13	203.63	75.49	1.14	6.53	12.15	34.4	45.64	1.43	4.39	8.71	12.37
14-center hole	203.78	75.04	1.13	5.42	12.66				1.88	7.07	12.38
15-offset hole	203.48	75.12	1.08	4.91	5.06				3.68	22.36	15.87
16	203.61	75.21	1.14	6.61	1.69	33.48	44.93	3.31	0.6	3.55	2.02
17-center hole	203.47	75.04	1.12	5.52	4.71				0.32	2.55	2.69
18-offset hole	203.54	75.37	1.09	5.1	6.78				1.02	20	5.89
19	254.17	99.89	1.14	5.83	34.73	47.6	51.97	6.07	0.29	14.21	3.42
20-center hole	253.88	99.99	1.1	4.72	16.07				0.54	16.72	16.89
21-offset hole	253.87	99.94	1.09	4.41	27.89				2.88	17.1	14.44
22	253.87	99.98	1.14	5.95	19.41	47.16	51.6	0.75	4.77	2.78	4.73
23-center hole	253.86	100.05	1.09	4.86	1.37				1.26	0.32	13.68
24-offset hole	253.75	99.86	1.07	4.36	0.67				6.37	0.26	3.23
25	253.55	99.92	1.14	6.09	7.87	46.89	51.4	2.92	7.72	3.22	7.54
26-center hole	253.61	100	1.12	4.97	6.15				10.37	3.24	0.1
27-offset hole	253.14	100.02	1.09	4.64	1.68				9.05	2.11	0.62
Average					7.8	36.45	43.72	3.79	4.94	11.41	10.32
Cov					8.27	8.18	7.52	2.23	3.37	7.43	6.6

Table 5 Comparison of DBN, BPN and Paddle model

Method	Training data			Validation data			Testing data		
	R^*	MSE	MAE	R^*	MSE	MAE	R^*	MSE	MAE
DBN	0.99	1.79	0.81	0.99	1.70	0.81	0.99	1.92	0.84
BPN	0.85	3.27	1.70	0.83	3.21	2.11	0.81	4.97	2.74
Paddle	0.83	3.11	1.66	0.84	2.57	1.87	0.85	4.77	2.55

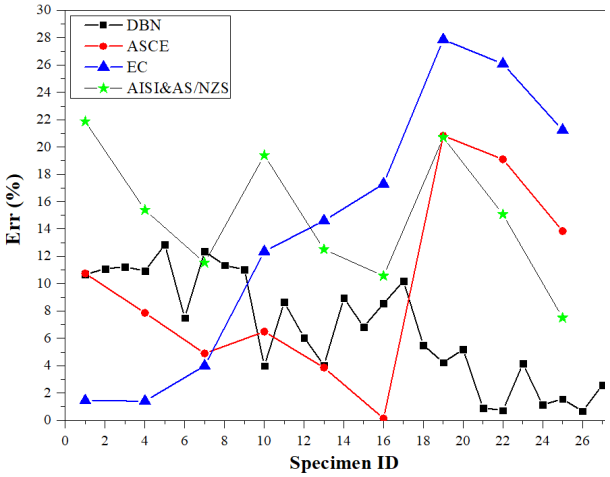

(a) DBN, ASCE, EC and AISI&AS/NZS for unfastened sections

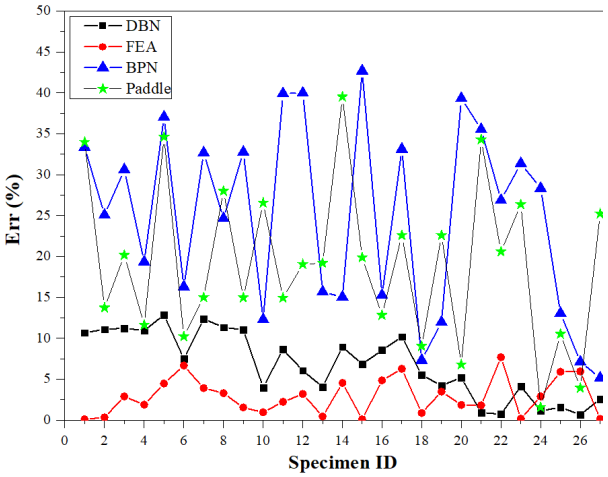

(b) DBN, FEA, BPN and Paddle for unfastened sections

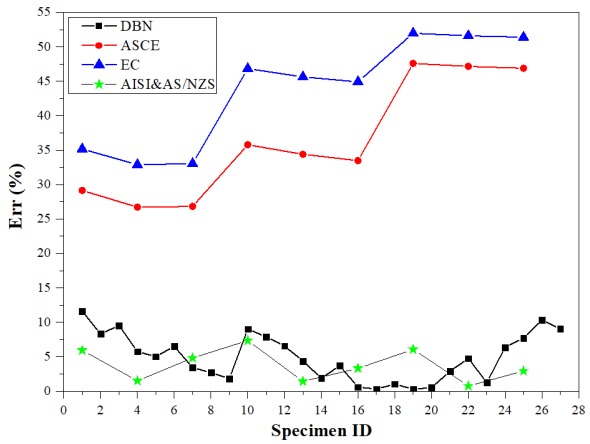

(c) DBN, ASCE, EC and AISI&AS/NZS for fastened sections

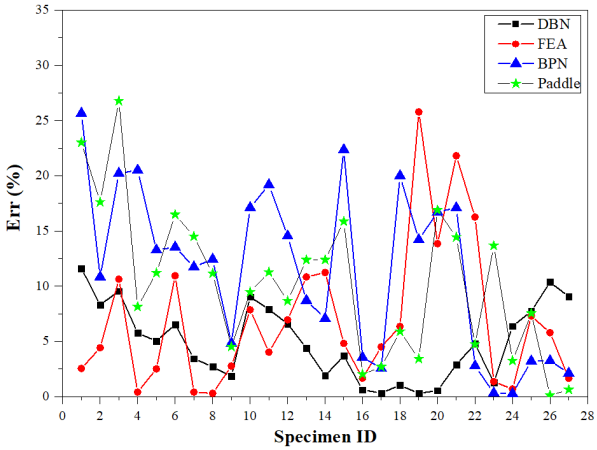

(d) DBN, FEA, BPN and Paddle for fastened sections

Fig.7 Absolute percentage error for various methods

6 Parametric study

Thorough parametric research was performed using DBN predictions. The effects of section size, web holes, and bearing length on the web crippling strength of cold-formed stainless steel perforated channels are investigated qualitatively and quantitatively.

6.1 Effect of r/t, N/t, h/t, fastened flanges and b/t

The *r/t* ratio has a negative impact on the P_n of cold-formed stainless steel channels, as demonstrated in Figs.8(a-c). When the *r/t* ratio was increased from 0.48 to 12, the P_n of cold-formed stainless steel channels was reduced significantly (by 95%). From Figs.8(d-f), it can

be seen that FEA results show the same pattern as DBN results in terms of the effect of *r/t* on web crippling strength of cold-formed stainless steel channels.

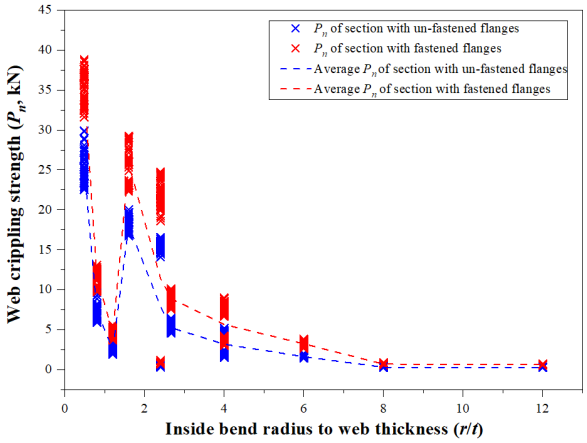

(a) Sections with ferritic stainless steel using DBN results

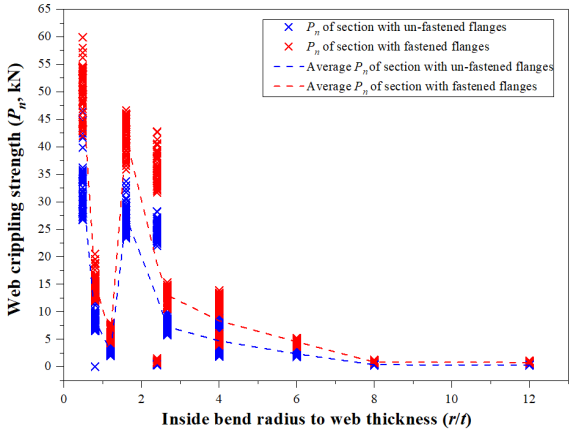

(b) Sections with duplex stainless steel using DBN results

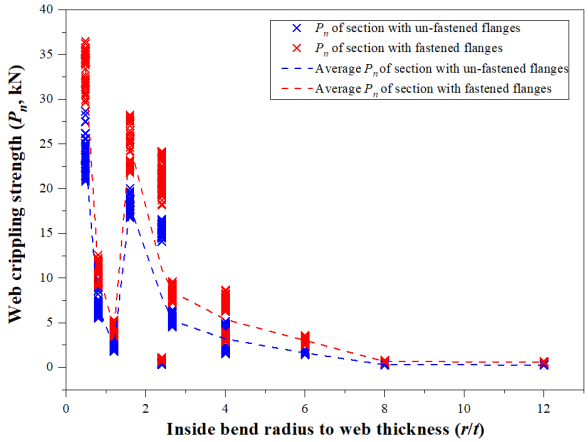

(c) Sections with austenitic stainless steel using DBN results

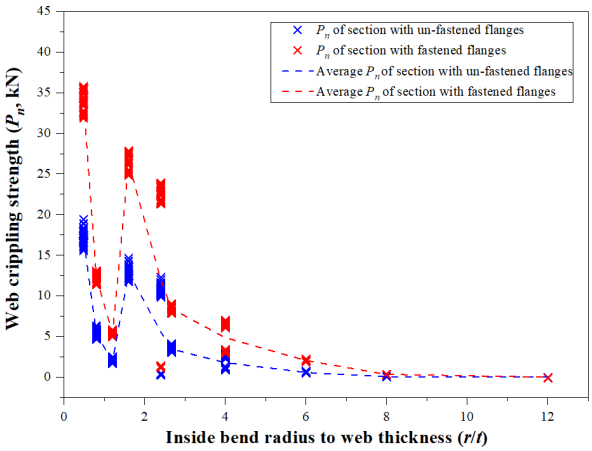

(d) Sections with ferritic stainless steel using FEA results

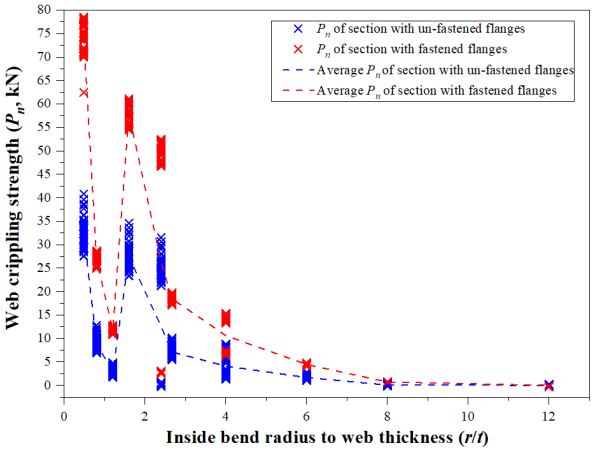

(e) Sections with duplex stainless steel using FEA results

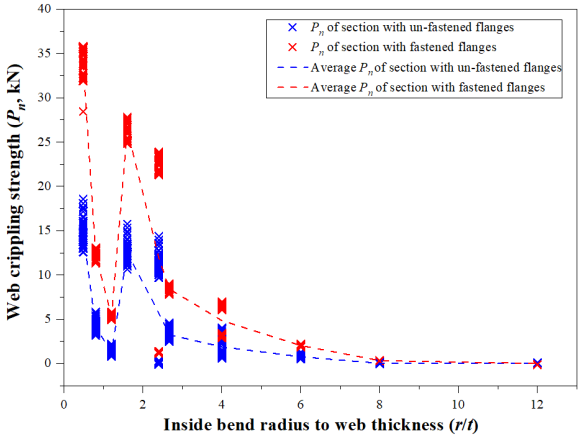

(f) Sections with austenitic stainless steel using FEA results

Fig.8 Effect of *r*/*t*

311 Fig.9 depicts the effect of the *N/t* ratio on the P_n. When the ratio (*N/t*) was increased
312 from 20 to 200, the P_n was reduced. The reduced percentages of P_n for unfastened sections of
313 cold-formed ferritic, duplex, and austenitic stainless steel are 98.28%, 98.63%, and 98.17%,
314 respectively while the values for fastened sections are 97.19%, 97.88%, and 97.26%.

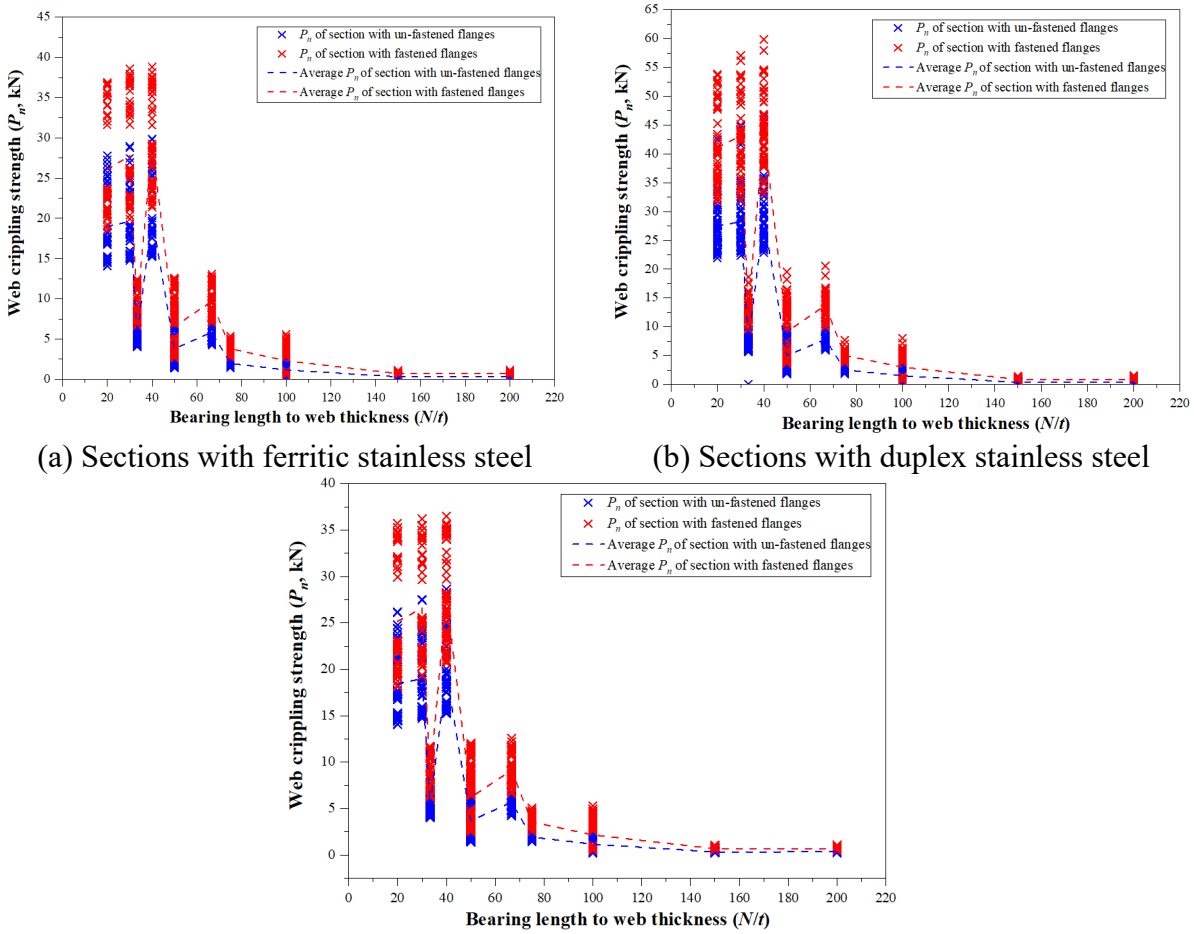

(a) Sections with ferritic stainless steel (b) Sections with duplex stainless steel

(c) Sections with austenitic stainless steel

Fig.9 Effect of *N/t*

315 The decreasing trend of P_n as the *h/t* ratio was increased is shown in Fig.10. For cold-
316 formed ferritic, duplex, and austenitic grades of stainless steel, the average P_n of unfastened
317 sections was reduced by 98.29 %, 98.70 %, and 98.18 %, respectively, as the *h/t* ratio
318 increases from 38.2 to 570.2, and the values of fastened sections are 97.18 %, 97.92 %, and
319 97.23 %.

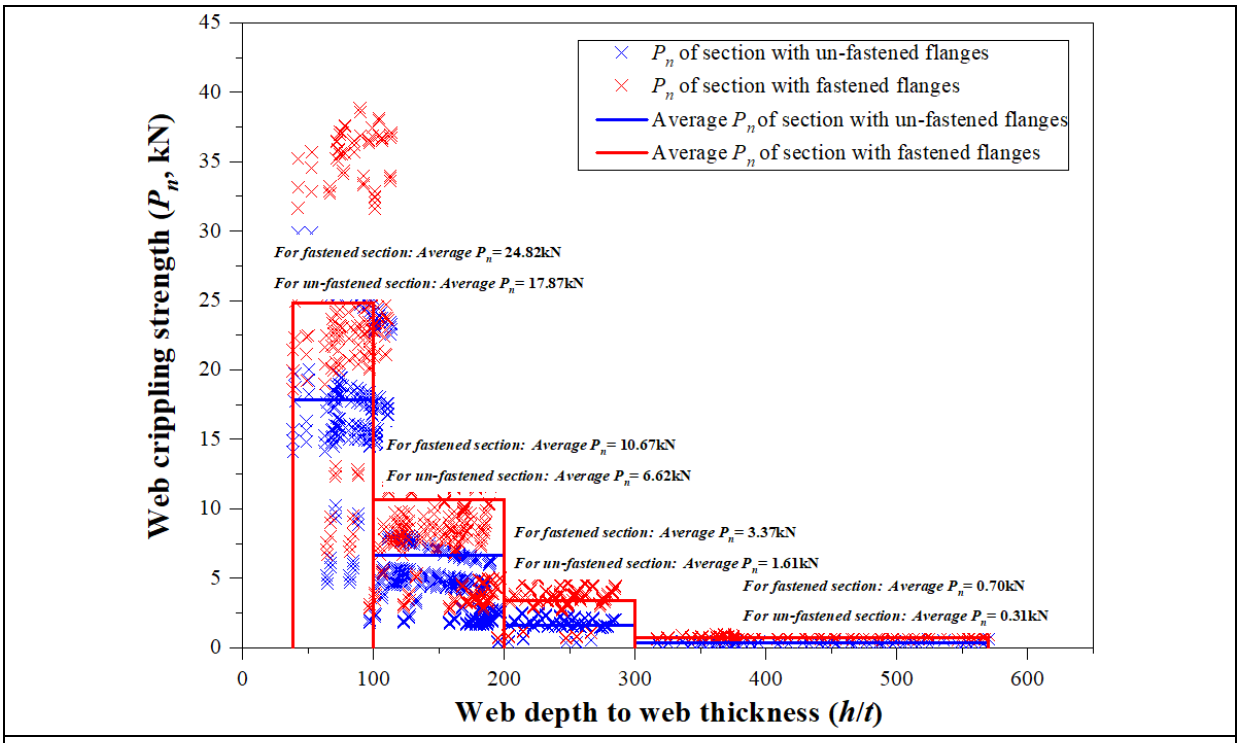

(a) Sections with ferritic stainless steel

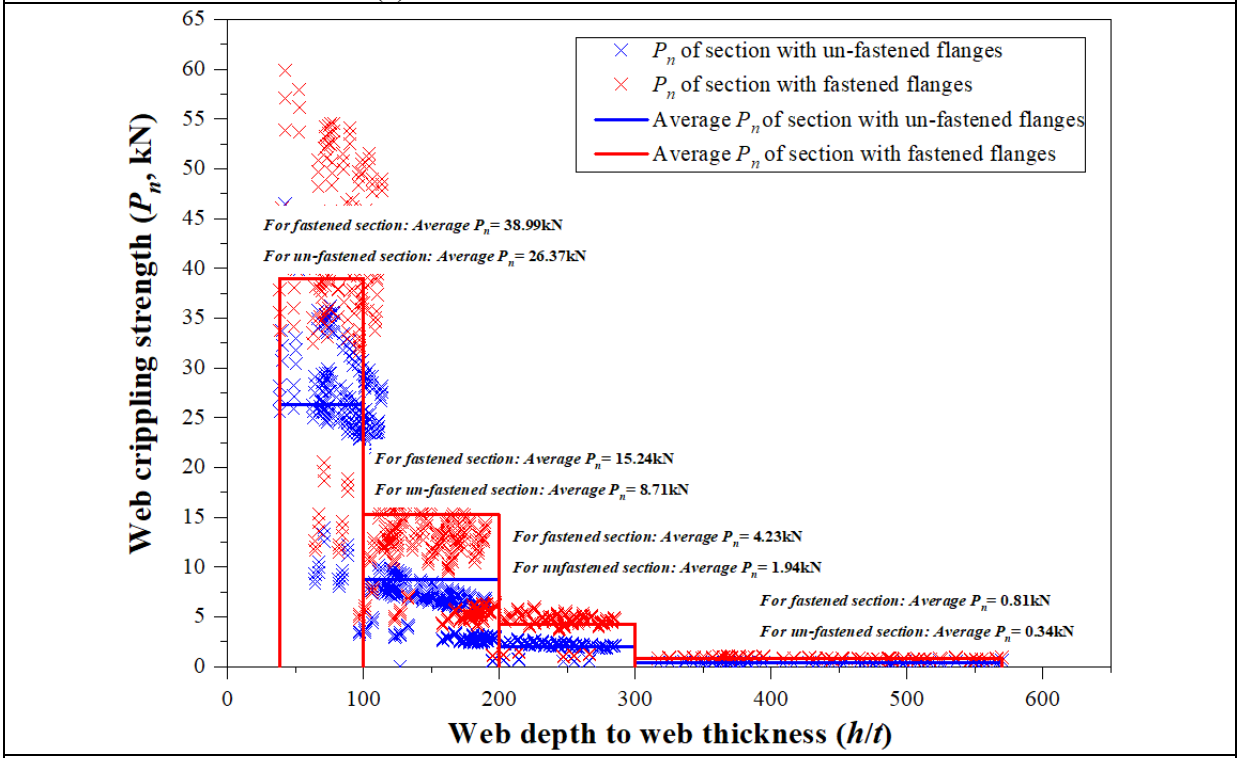

(b) Sections with duplex stainless steel

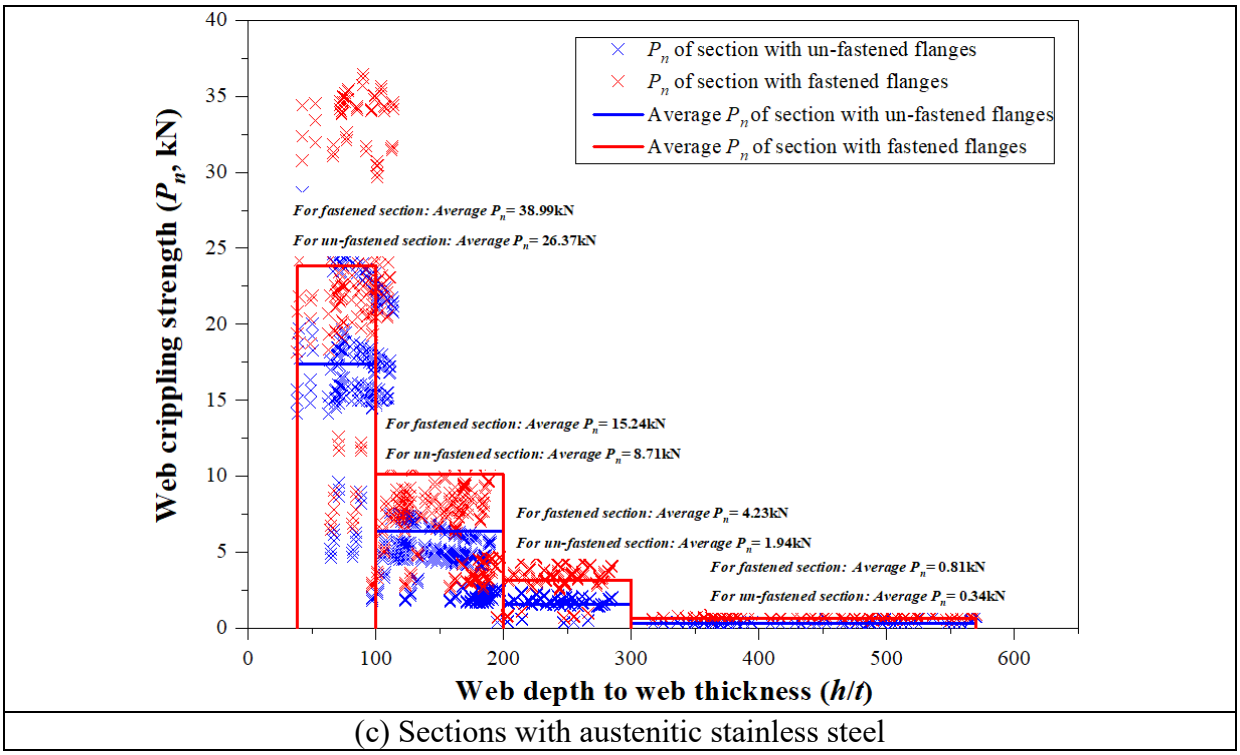

(c) Sections with austenitic stainless steel

Fig.10 Effect of h/t

According to Figs.8-10, the average P_n of fastened sections is 50.88%, 60.47%, and 48.23% greater than unfastened sections for cold-formed ferritic, duplex, and austenitic stainless steel, respectively.

As shown in Figs.11(a) and 11(b), P_n for unlipped and lipped unfastened sections is nearly identical. For cold-formed ferritic, duplex, and austenitic grades of stainless steel, the difference is significant, with average ratios of P_n for the investigated channels of 1.113, 1.116, and 1.120, respectively. As the b_l/t ratio increases, the P_n of fastened sections decreases, as illustrated in Fig.10(c). When the b_l/t ratio increased from 5.2 to 92.0, the P_n of ferritic, duplex and austenitic grades of stainless steel channels declined by 95.42%, 96.49 %, and 95.47%, respectively.

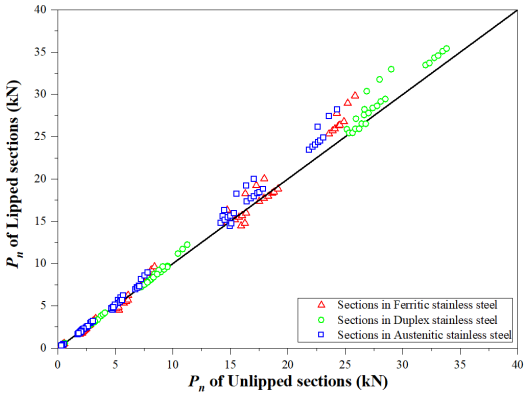

(a) Comparison of lipped and unlipped sections with unfastened flanges

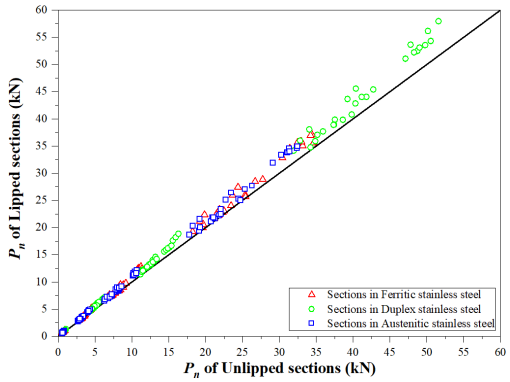

(b) Comparison of lipped and unlipped sections with fastened flanges

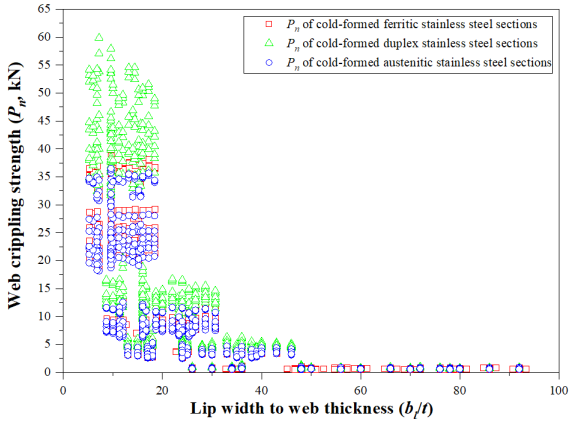

(c) Web crippling strength of fastened sections

Fig.11 Effect of b_l/t

6.2 Effect of a/h, N/h and fastened flanges

There is a declining trend in R when the a/h ratio rises from 0.2 to 0.6, as illustrated in Fig.12. The R for centered-hole sections with unfastened and fastened flanges is similar, and the average R for these sections decreases from 0.96 to 0.75 when the ratio a/h goes from 0.2 to 0.6. In contrast, the R for the offset-hole sections with unfastened and fastened flanges, differ dramatically. Table 6 reveals that the average R for offset-hole sections with unfastened flanges decreased from 0.93 to 0.67. The R for sections with fastened flanges decreased from 0.94 to 0.77 when the a/h ratio was changed from 0.2 to 0.6.

Table 6 Average web crippling strength reduction factor (R)

Section type / Web hole		Ferritic		Duplex		Austenitic	
		Unfastened sections	Fastened sections	Unfastened sections	Fastened sections	Unfastened sections	Fastened sections
Center hole with a/h at	0.2	0.96	0.96	0.96	0.96	0.96	0.96
	0.4	0.87	0.87	0.88	0.88	0.87	0.87
	0.6	0.76	0.74	0.78	0.75	0.75	0.73
Offset hole with a/h at	0.2	0.93	0.94	0.93	0.94	0.93	0.94
	0.4	0.80	0.86	0.80	0.86	0.80	0.86
	0.6	0.67	0.77	0.67	0.77	0.67	0.77

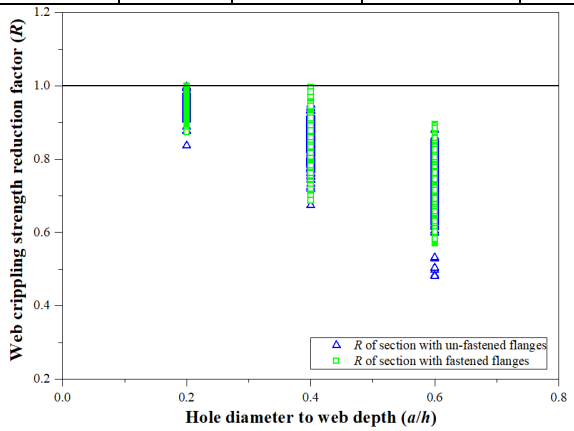

(a) Center-hole sections with ferritic stainless steel

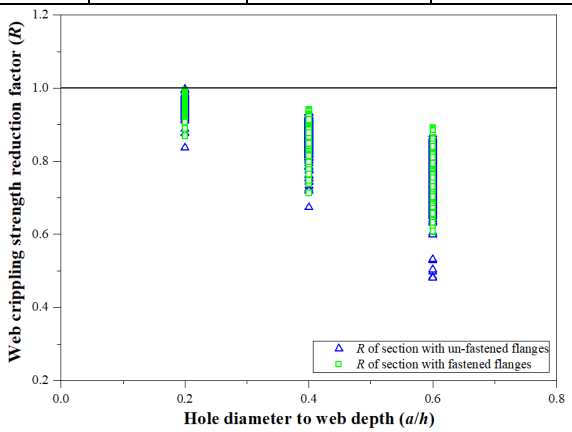

(b) Center-hole sections with ferritic stainless steel duplex stainless steel

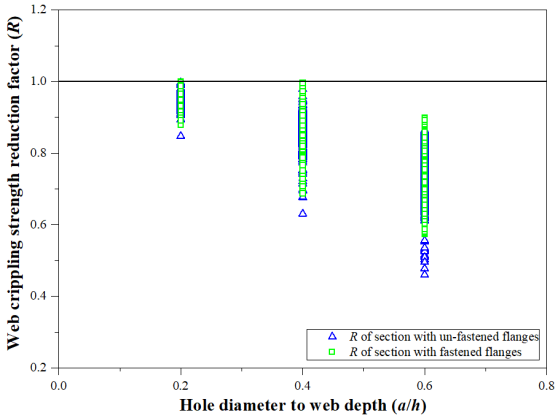

(c) Center-hole sections with ferritic stainless steel austenitic stainless steel

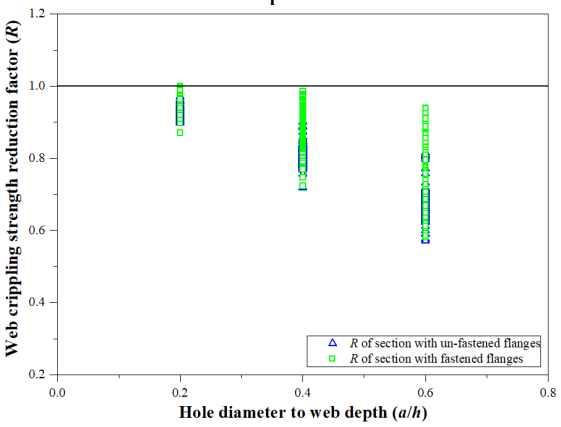

(d) Offset-hole sections with ferritic stainless steel

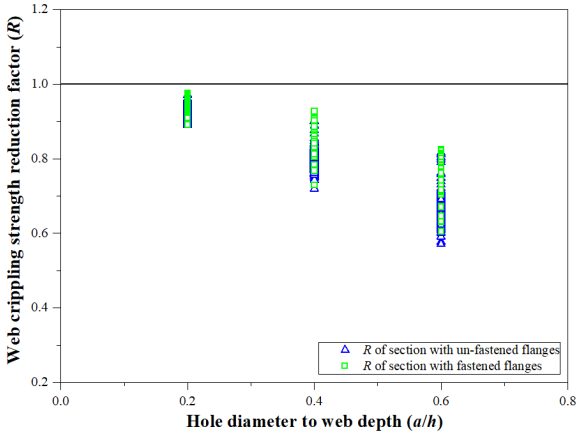

(e) Offset-hole sections with duplex stainless steel

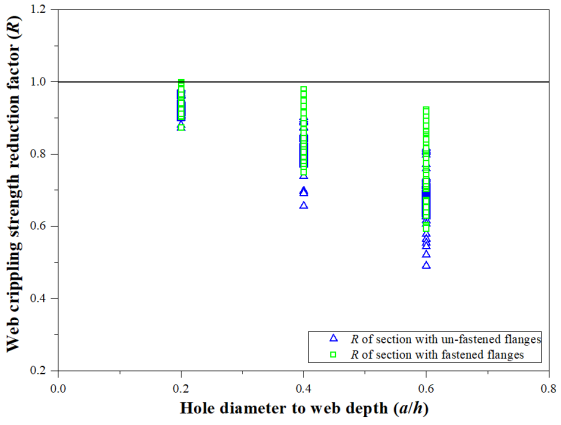

(f) Offset-hole sections with austenitic stainless steel

Fig.12 Effect of a/h

The average R for cold-formed stainless steel sections changed by 5% when the ratio of N/h changed from 0.18 to 1.05.

Fig.13 and Table 6 show that the average R for different stainless steel materials varies slightly (Ferritic, Duplex, and Austenitic). For the sections with centered web holes, there is little difference in the average R of sections with both unfastened and fastened flanges, while the average values of R for fastened sections with offset web holes are 7.5% higher than those with unfastened flanges.

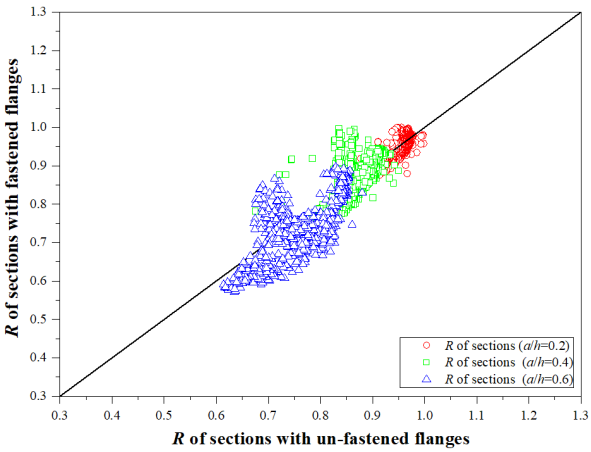

(a) Center-hole sections with ferritic stainless steel

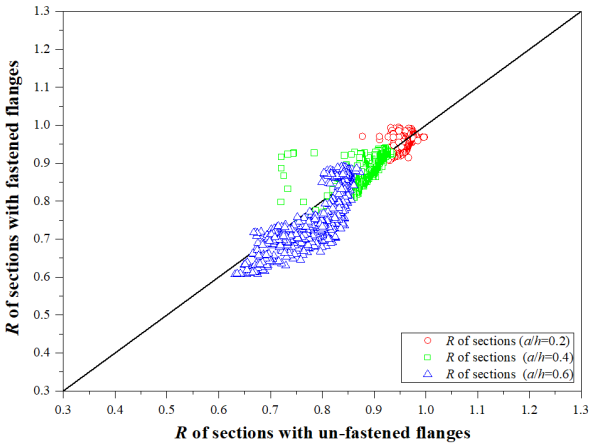

(b) Center-hole sections with duplex stainless steel

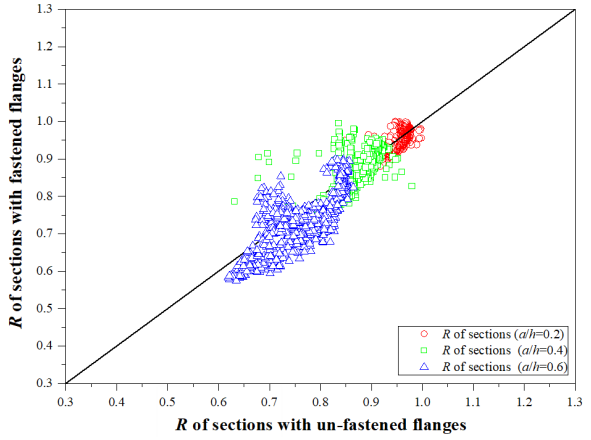

(c) Center-hole sections with austenitic stainless steel

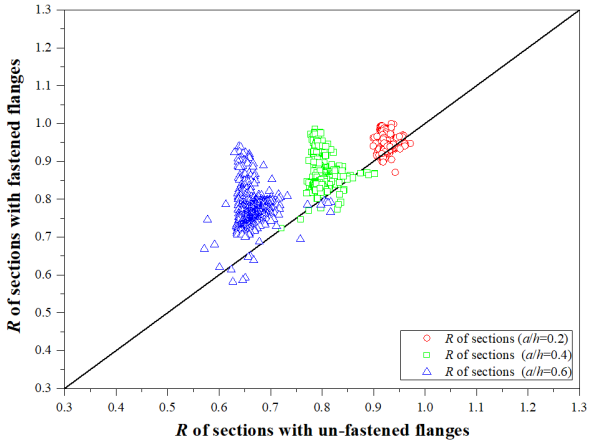

(d) Offset-hole sections with ferritic stainless steel

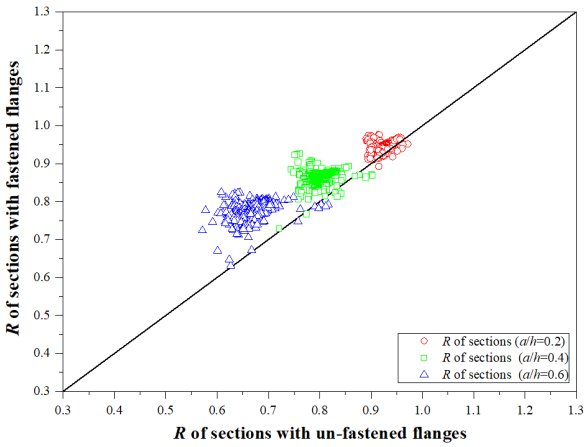

(e) Offset-hole sections with duplex stainless steel

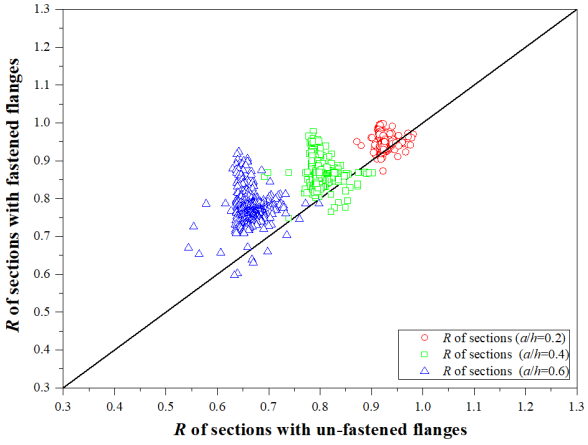

(f) Offset-hole sections with austenitic stainless steel

Fig.13 Effect of fastened flanges

7 Proposed design equations

Using the regression analysis software SPSS [44], DBN predictions were used to propose new equations for cold-formed stainless steel perforated channels in the form of web crippling strength and web crippling strength reduction factors. Limitations for proposed design equations are: $h/t \leq 600$, $N/t \leq 200$, $R/t \leq 12.0$, $N/h \leq 1.15$, and $a/h \leq 0.6$.

7.1 Proposed equations

Web crippling strength (P_{prop}) of cold-formed stainless steel unlipped and lipped plain channels are given:

For unfastened sections,

$$P_{prop} = Ct^2 f_y (1 - C_R \sqrt{\frac{r}{t}})(1 + C_N \sqrt{\frac{N}{t}})(1 - C_h \sqrt{\frac{h}{t}}) > 0 \quad (26)$$

For fastened sections,

$$P_{prop} = Ct^2 f_y (1 - C_R \sqrt{\frac{R}{t}})(1 + C_N \sqrt{\frac{N}{t}})(1 - C_h \sqrt{\frac{h}{t}})(1 + C_l \sqrt{\frac{b_l}{t}}) > 0 \quad (27)$$

Where, the recommended values for C, C_R, C_N, C_h and C_l are given in Table 7.

Table 7 Coefficients for cold-formed stainless steel channel for ITF loading case

Section type	Stainless steel type	C	C_R	C_N	C_h	C_l
Unfastened lipped sections	Ferritic	19.243	0.335	0.041	0.029	0.001
	Duplex	19.763	0.237	0.041	0.047	0.001
	Austenitic	18.882	0.304	0.039	0.030	0.001
Fastened lipped sections	Ferritic	23.968	0.306	0.063	0.001	0.016
	Duplex	21.598	0.244	0.042	0.028	0.022
	Austenitic	24.112	0.298	0.053	0.002	0.014
Unfastened unlipped sections	Ferritic	19.243	0.335	0.041	0.029	--
	Duplex	19.763	0.237	0.041	0.047	--
	Austenitic	18.882	0.304	0.039	0.030	--
Fastened unlipped sections	Ferritic	16.181	0.293	0.066	0.001	--
	Duplex	13.724	0.250	0.028	0.006	--
	Austenitic	15.882	0.288	0.058	0.001	--

The web crippling strength reduction factor (R_{prop}) of cold-formed stainless steel perforated channels are given:

For sections with a centered hole,

$$R_{prop} = \alpha - \gamma \frac{a}{h} + \lambda \frac{N}{h} \leq 1 \tag{28}$$

For sections with an offset hole,

$$R_{prop} = \beta - \mu \frac{a}{h} + \zeta \frac{N}{h} + \xi \frac{x}{h} \leq 1 \tag{29}$$

Where, the recommended values for α, γ, λ, β, μ, ζ and ξ are given in Table 8.

Table 8 Coefficients for proposed equations on web crippling strength reduction factor

Stainless steel grade		Unfastened section	Fastened section
Ferritic	α	1.069	1.046
	γ	0.521	0.474
	λ	0.010	0.033
	β	0.530	0.938
	μ	0.090	0.557
	ζ	0.130	0.081
	ξ	0.660	0.127
Duplex	α	1.066	1.046
	γ	0.487	0.428
	λ	0.010	0.014
	β	0.944	1.019
	μ	0.368	0.610
	ζ	0.044	0.059
	ξ	0.105	0.027
Austenitic	α	1.064	1.047
	γ	0.526	0.480
	λ	0.024	0.036
	β	0.620	0.983
	μ	0.150	0.585
	ζ	0.117	0.069
	ξ	0.535	0.070

The prediction accuracy of the proposed equations was assessed by comparing the proposed design strengths to the failure loads obtained from the FFA and results obtained from the proposed equations of Yousefi et al. [12-13] and Uzzaman et al. [35-37]. As shown in Tables 9 and 10, the reduced web crippling strengths calculated from the proposed equations are highly predictive of the numerical failure loads, and the average values of the ratios P/P_{prop} and R/R_{prop} are close to 1, which confirms the accurate prediction capability of the proposed equations for calculating the ITF web crippling strengths of cold-formed stainless steel perforated channels. Besides, Yousefi et al [12-13] and Uzzaman et al. [35-37] proposed the equations for cold-formed ferritic stainless steel unlipped channels and cold-formed carbon steel lipped channels, respectively. However, the investigated sections in Yousefi et al [12-13] and Uzzaman et al. [35-37] are ferritic unlipped channels and carbon steel channels. Unlike their proposed equations, the effects of different types of stainless steel

and lips on web crippling strength were included in the proposed equations of the current study. Therefore, from Tables 9 and 10, it can be found that the proposed equations in this study outperformed the proposed equations from other sources [12-13. 35-37]. It is noted that the specimen labelling in Tables 9 and 10 follows the format of Yousefi et al. [12-13].

Table 9 Web crippling strength obtained from FEA, current design guidelines and proposed equations

(a) Unfastened sections

Specimen	P_{FEA} (kN)	P_{FEA}/P_{ASCE}	P_{FEA}/P_{EC}	$P_{FEA}/P_{AISI\&AS/NZS}$	P_{FEA}/P_{prop}
Unlipped cold-formed ferritic stainless steel [12-13]					
175×60-t1.2-N50-A0-FR	4.16	1.13	0.93	1.01	0.99
175×60-t4.0-N50-A0-FR	67.03	0.94	0.72	0.84	1.01
175×60-t6.0-N50-A0-FR	135.73	0.81	0.62	0.72	0.86
175×60-t1.2-N75-A0-FR	4.31	1.17	0.96	1.05	0.99
175×60-t4.0-N75-A0-FR	69.27	0.96	0.74	0.86	1.02
175×60-t6.0-N75-A0-FR	144.78	0.86	0.66	0.76	0.89
175×60-t1.2-N100-A0-FR	4.49	1.19	0.97	1.06	0.99
175×60-t4.0-N100-A0-FR	72.93	1.00	0.78	0.90	1.05
175×60-t6.0-N100-A0-FR	151.45	0.89	0.68	0.80	0.92
200×75-t1.2-N50-A0-FR	3.52	1.22	1.00	1.09	0.89
200×75-t4.0-N50-A0-FR	68.76	1.16	0.76	0.88	1.05
200×75-t6.0-N50-A0-FR	140.57	1.00	0.65	0.76	0.90
200×75-t1.2-N75-A0-FR	3.65	0.97	1.04	1.13	0.88
200×75-t4.0-N75-A0-FR	70.89	1.08	0.78	0.90	1.06
200×75-t6.0-N75-A0-FR	150.99	0.99	0.69	0.81	0.94
200×75-t1.2-N100-A0-FR	4.16	0.98	1.03	1.12	0.95
200×75-t4.0-N100-A0-FR	74.01	1.04	0.80	0.93	1.08
200×75-t6.0-N100-A0-FR	156.29	0.95	0.72	0.83	0.96
250×100-t4.0-N50-A0-FR	69.95	1.23	0.81	0.93	1.11
250×100-t6.0-N50-A0-FR	145.04	1.08	0.69	0.80	0.95
250×100-t4.0-N75-A0-FR	71.95	1.15	0.82	0.95	1.11
250×100-t6.0-N75-A0-FR	157.77	1.07	0.75	0.87	1.01
250×100-t4.0-N100-A0-FR	74.88	1.11	0.85	0.98	1.13
250×100-t6.0-N100-A0-FR	161.18	1.02	0.76	0.88	1.01
Average		1.04	0.80	0.91	0.99
Cov		0.11	0.12	0.11	0.08
Lipped cold-formed ferritic stainless steel					
110×74×33-t1.5-N50-A0-FR	6.49	1.14	0.78	0.59	1.10
110×74×33-t1.5-N75-A0-FR	6.82	1.05	0.80	0.56	1.11
110×74×33-t1.5-N100-A0-FR	7.16	1.01	0.82	0.55	1.13
200×74×33-t1.5-N50-A0-FR	5.18	1.11	0.80	0.47	0.99
200×74×33-t1.5-N75-A0-FR	5.33	1.01	0.80	0.44	0.98
200×74×33-t1.5-N100-A0-FR	5.48	0.94	0.81	0.42	0.98
Average		1.04	0.80	0.51	1.05
Cov		0.07	0.01	0.06	0.07
Lipped cold-formed duplex stainless steel					
110×74×33-t1.5-N50-A0-FR	12.55	1.00	0.89	0.52	1.04
110×74×33-t1.5-N75-A0-FR	13.25	0.93	0.92	0.50	1.06
110×74×33-t1.5-N100-A0-FR	13.94	0.89	0.95	0.49	1.07
200×74×33-t1.5-N50-A0-FR	8.70	0.85	0.79	0.36	0.94
200×74×33-t1.5-N75-A0-FR	8.99	0.77	0.80	0.34	0.94

200×74×33-t1.5-N100-A0-FR	9.27	0.73	0.81	0.32	0.93
Average		0.86	0.86	0.42	1.00
Cov		0.09	0.06	0.08	0.06
Lipped cold-formed austenitic stainless steel					
110×74×33-t1.5-N50-A0-FR	6.06	1.06	0.73	0.55	1.08
110×74×33-t1.5-N75-A0-FR	6.38	0.99	0.75	0.53	1.09
110×74×33-t1.5-N100-A0-FR	6.71	0.94	0.77	0.51	1.11
200×74×33-t1.5-N50-A0-FR	4.76	1.02	0.73	0.44	0.96
200×74×33-t1.5-N75-A0-FR	4.91	0.93	0.74	0.41	0.95
200×74×33-t1.5-N100-A0-FR	5.06	0.87	0.75	0.39	0.95
Average		0.97	0.75	0.47	1.02
Cov		0.06	0.01	0.06	0.07

(b) Fastened sections

Specimen	P_{FEA} (kN)	P_{FEA}/P_{ASCE}	P_{FEA}/P_{EC}	$P_{FEA}/P_{AISI\&AS/NZS}$	P_{FEA}/P_{prop}
Unlipped cold-formed ferritic stainless steel [12-13]					
175×60-t1.2-N50-A0-FR	6.52	0.95	1.45	1.58	0.99
175×60-t4.0-N50-A0-FR	75.52	0.86	0.82	0.94	1.00
175×60-t6.0-N50-A0-FR	149.45	0.74	0.68	0.79	0.88
175×60-t1.2-N75-A0-FR	6.79	0.91	1.43	1.56	0.97
175×60-t4.0-N75-A0-FR	87.83	0.95	0.94	1.09	1.11
175×60-t6.0-N75-A0-FR	174.15	0.83	0.79	0.92	0.99
175×60-t1.2-N100-A0-FR	6.94	0.88	1.43	1.56	0.94
175×60-t4.0-N100-A0-FR	94.05	0.98	1.00	1.15	1.15
175×60-t6.0-N100-A0-FR	190.26	0.88	0.86	1.00	1.05
200×75-t1.2-N50-A0-FR	6.32	0.96	1.61	1.74	0.96
200×75-t4.0-N50-A0-FR	76.28	0.88	0.84	0.97	1.01
200×75-t6.0-N50-A0-FR	150.97	0.76	0.70	0.81	0.89
200×75-t1.2-N75-A0-FR	6.63	0.93	1.60	1.73	0.95
200×75-t4.0-N75-A0-FR	89.75	0.99	0.98	1.13	1.14
200×75-t6.0-N75-A0-FR	175.95	0.85	0.81	0.94	1.00
200×75-t1.2-N100-A0-FR	6.69	0.89	1.57	1.70	0.90
200×75-t4.0-N100-A0-FR	93.45	0.99	1.02	1.17	1.15
200×75-t6.0-N100-A0-FR	181.89	0.85	0.83	0.97	1.00
250×100-t4.0-N50-A0-FR	75.93	0.91	0.88	1.01	1.01
250×100-t6.0-N50-A0-FR	152.61	0.79	0.73	0.84	0.90
250×100-t4.0-N75-A0-FR	90.01	1.03	1.03	1.19	1.14
250×100-t6.0-N75-A0-FR	177.27	0.88	0.84	0.98	1.01
250×100-t4.0-N100-A0-FR	100.81	1.11	1.15	1.32	1.24
250×100-t6.0-N100-A0-FR	200.01	0.96	0.94	1.09	1.10
Average		0.91	1.04	1.18	1.02
Cov		0.08	0.30	0.30	0.09
Lipped cold-formed ferritic stainless steel					
110×74×33-t1.5-N50-A0-FR	12.28	1.34	1.47	1.33	1.08
110×74×33-t1.5-N75-A0-FR	12.55	1.28	1.47	1.27	1.04
110×74×33-t1.5-N100-A0-FR	13.06	1.26	1.50	1.25	1.03

200×74×33-t1.5-N50-A0-FR	12.38	1.55	1.91	1.56	1.07
200×74×33-t1.5-N75-A0-FR	12.42	1.45	1.87	1.46	1.01
200×74×33-t1.5-N100-A0-FR	12.48	1.38	1.85	1.39	0.97
Average		1.38	1.68	1.38	1.03
Cov		0.10	0.20	0.11	0.04
Lipped cold-formed duplex stainless steel					
110×74×33-t1.5-N50-A0-FR	18.67	0.93	1.32	0.94	1.07
110×74×33-t1.5-N75-A0-FR	19.56	0.91	1.35	0.92	1.07
110×74×33-t1.5-N100-A0-FR	20.50	0.90	1.39	0.91	1.09
200×74×33-t1.5-N50-A0-FR	16.19	0.92	1.47	0.93	1.02
200×74×33-t1.5-N75-A0-FR	16.48	0.88	1.47	0.89	0.99
200×74×33-t1.5-N100-A0-FR	16.74	0.84	1.46	0.85	0.97
Average		0.90	1.41	0.91	1.04
Cov		0.03	0.06	0.03	0.04
Lipped cold-formed austenitic stainless steel					
110×74×33-t1.5-N50-A0-FR	11.69	1.28	1.40	1.07	1.07
110×74×33-t1.5-N75-A0-FR	12.04	1.23	1.41	1.00	1.05
110×74×33-t1.5-N100-A0-FR	12.57	1.21	1.45	0.96	1.05
200×74×33-t1.5-N50-A0-FR	11.56	1.45	1.78	1.06	1.05
200×74×33-t1.5-N75-A0-FR	11.59	1.35	1.75	0.96	1.00
200×74×33-t1.5-N100-A0-FR	11.65	1.29	1.72	0.89	0.96
Average		1.30	1.59	0.99	1.03
Cov		0.08	0.17	0.06	0.04

Table 10 Web crippling strength reduction factors obtained from various methods

(a) Unfastened sections

Specimen	P_{A0}(kN)	Reduction factor $R=P_u/P_{A0}$		Reduction factor $R_{Yousefi}$ by Yousefi [12-13,9]		Reduction factor R by Uzzaman et al. [27-29]		Reduction factor R_{prop} by Equation		$R/R_{Yousefi}$		$R/R_{Uzzaman}$		R/R_{prop}	
		Center hole	Offset hole	Center hole	Offset hole	Center hole	Offset hole	Center hole	Offset hole	Center hole	Offset hole	Center hole	Offset hole	Center hole	Offset hole
Unlipped sections with ferritic stainless steel [12-13]															
175×60-t1.2-N50-A0.2-FR	4.16	0.96	0.92	0.87	0.94	0.94	--	0.96	0.93	1.10	0.98	0.86	--	1.00	0.99
175×60-t1.2-N75-A0.2-FR	4.31	0.96	0.96	0.88	0.93	0.95	--	0.97	0.93	1.09	1.03	0.88	--	0.99	1.03
175×60-t1.2-N75-A0.4-FR	4.31	0.88	0.88	0.75	0.79	0.84	--	0.87	0.81	1.17	1.12	0.90	--	1.01	1.09
175×60-t1.2-N100-A0.2-FR	4.49	0.96	0.96	0.89	0.93	0.95	--	0.97	0.94	1.08	1.04	0.90	--	0.99	1.02
175×60-t1.2-N100-A0.4-FR	4.49	0.88	0.87	0.76	0.78	0.84	--	0.88	0.82	1.16	1.11	0.91	--	1.00	1.07
200×75-t6.0-N50-A0.2-FR	140.57	0.94	0.94	0.87	0.95	0.94	--	0.96	0.93	1.08	0.99	0.86	--	0.98	1.01
200×75-t6.0-N50-A0.4-FR	140.57	0.80	0.83	0.74	0.80	0.84	--	0.87	0.80	1.08	1.04	0.88	--	0.92	1.03
200×75-t4.0-N100-A0.2-FR	74.01	0.93	0.92	0.89	0.93	0.95	--	0.97	0.94	1.05	0.99	0.89	--	0.96	0.98
200×75-t4.0-N100-A0.4-FR	74.01	0.82	0.81	0.76	0.79	0.84	--	0.87	0.81	1.08	1.03	0.90	--	0.94	1.00
250×100-t6.0-N50-A0.2-FR	145.04	0.96	0.90	0.86	0.95	0.94	--	0.96	0.92	1.11	0.95	0.86	--	1.00	0.98
250×100-t6.0-N50-A0.4-FR	145.04	0.82	0.79	0.73	0.80	0.84	--	0.86	0.80	1.12	0.98	0.87	--	0.95	0.99
250×100-t4.0-N100-A0.2-FR	74.88	0.92	0.90	0.88	0.93	0.95	--	0.96	0.93	1.05	0.96	0.88	--	0.95	0.97
250×100-t4.0-N100-A0.4-FR	74.88	0.80	0.79	0.75	0.79	0.84	--	0.87	0.81	1.07	1.00	0.90	--	0.92	0.98
Average										1.10	1.02	0.88	--	0.97	1.01
Cov										0.04	0.05	0.02	--	0.03	0.04
Lipped sections with ferritic stainless steel															
110×74×33-t1.5-N50-A0.2-FR	6.49	0.93	0.92	0.88	0.93	0.95	--	0.97	0.94	1.05	0.99	0.89	--	0.96	0.99
110×74×33-t1.5-N75-A0.2-FR	6.82	0.94	0.93	0.90	0.92	0.95	--	0.98	0.95	1.04	1.01	0.91	--	0.96	0.98
110×74×33-t1.5-N100-A0.2-FR	7.16	0.95	0.93	0.92	0.91	0.95	--	0.98	0.96	1.03	1.03	0.93	--	0.96	0.97
200×74×33-t1.5-N50-A0.4-FR	5.18	0.82	0.79	0.74	0.80	0.84	--	0.87	0.80	1.11	0.99	0.88	--	0.95	0.98
200×74×33-t1.5-N75-A0.4-FR	5.33	0.83	0.80	0.75	0.79	0.84	--	0.87	0.81	1.11	1.01	0.89	--	0.95	0.99
200×74×33-t1.5-N100-A0.4-FR	5.48	0.83	0.81	0.76	0.78	0.84	--	0.87	0.81	1.10	1.03	0.91	--	0.95	0.99
Average						0.89	--			1.07	1.01	0.90	--	0.96	0.98
Cov						0.06	--			0.03	0.02	0.02	--	0.01	0.01
Lipped sections with duplex stainless steel															
110×74×33-t1.5-N50-A0.2-FR	6.49	0.94	0.93	0.88	0.93	0.95	--	0.97	0.94	1.06	1.00	0.92	--	0.97	0.99
110×74×33-t1.5-N75-A0.2-FR	6.82	0.94	0.94	0.90	0.92	0.95	--	0.98	0.95	1.05	1.02	0.92	--	0.97	0.99
110×74×33-t1.5-N100-A0.2-FR	7.16	0.95	0.94	0.92	0.91	0.95	--	0.98	0.96	1.03	1.04	0.92	--	0.96	0.98
200×74×33-t1.5-N50-A0.4-FR	5.18	0.86	0.79	0.74	0.80	0.84	--	0.87	0.80	1.17	0.99	0.94	--	1.00	0.99
200×74×33-t1.5-N75-A0.4-FR	5.33	0.86	0.80	0.75	0.79	0.84	--	0.87	0.81	1.16	1.01	0.95	--	0.99	0.99

200×74×33-t1.5-N100-A0.4-FR	5.48	0.87	0.80	0.76	0.78	0.84	--	0.87	0.81	1.15	1.03	0.95	--	0.99	0.99
Average						0.89	--			1.10	1.01	0.93	--	0.98	0.99
Cov						0.06	--			0.06	0.02	0.01	--	0.01	0.00
Lipped sections with austenitic stainless steel															
110×74×33-t1.5-N50-A0.2-FR	6.49	0.93	0.93	0.88	0.93	0.95	--	0.97	0.94	1.05	0.99	0.91	--	0.96	0.99
110×74×33-t1.5-N75-A0.2-FR	6.82	0.94	0.94	0.90	0.92	0.95	--	0.98	0.95	1.04	1.02	0.92	--	0.96	0.98
110×74×33-t1.5-N100-A0.2-FR	7.16	0.95	0.94	0.92	0.91	0.95	--	0.98	0.96	1.03	1.03	0.93	--	0.96	0.97
200×74×33-t1.5-N50-A0.4-FR	5.18	0.83	0.79	0.74	0.80	0.84	--	0.87	0.80	1.12	0.99	0.91	--	0.95	0.99
200×74×33-t1.5-N75-A0.4-FR	5.33	0.83	0.80	0.75	0.79	0.84	--	0.87	0.81	1.11	1.02	0.92	--	0.96	0.99
200×74×33-t1.5-N100-A0.4-FR	5.48	0.84	0.81	0.76	0.78	0.84	--	0.87	0.81	1.11	1.04	0.93	--	0.96	1.00
Average						0.89	--			1.08	1.01	0.92	--	0.96	0.99
Cov						0.06	--			0.04	0.02	0.01	--	0.00	0.01

(b) Fastened sections

Specimen	P_{A0}(kN)	Reduction factor $R=P_u/P_{A0}$		Reduction factor R by Yousefi [12-13,9]		Reduction factor R by Uzzaman et al. [27-29]		Reduction factor R by Equation		$R/R_{Yousefi}$		$R/R_{Uzzaman}$		R/R_{prop}	
		Center hole	Offset hole	Center hole	Offset hole	Center hole	Offset hole	Center hole	Offset hole	Center hole	Offset hole	Center hole	Offset hole	Center hole	Offset hole
Unlipped sections with ferritic stainless steel [12-13]															
175×60-t1.2-N50-A0.2-FR	6.52	0.95	0.94	0.99	1.00	0.93	--	0.96	0.94	0.96	0.94	1.03	--	0.99	1.00
175×60-t1.2-N75-A0.2-FR	6.79	0.95	0.93	1.00	0.99	0.93	--	0.97	0.94	0.95	0.94	1.02	--	0.98	0.99
175×60-t1.2-N75-A0.4-FR	6.79	0.84	0.84	0.99	0.87	0.83	--	0.87	0.85	0.85	0.97	1.01	--	0.96	0.99
175×60-t1.2-N100-A0.2-FR	6.94	0.95	0.94	1.00	0.98	0.94	--	0.97	0.93	0.95	0.96	1.01	--	0.98	1.01
175×60-t1.2-N100-A0.4-FR	6.94	0.84	0.85	0.99	0.86	0.84	--	0.88	0.85	0.85	0.99	1.00	--	0.96	1.00
200×75-t6.0-N50-A0.2-FR	150.97	0.99	1.00	0.99	1.00	0.92	--	0.96	0.95	1.00	1.00	1.07	--	1.03	1.05
200×75-t6.0-N50-A0.4-FR	150.97	0.86	0.99	0.98	0.88	0.82	--	0.87	0.87	0.88	1.12	1.05	--	0.99	1.14
200×75-t4.0-N100-A0.2-FR	93.45	0.93	0.95	1.00	0.99	0.94	--	0.97	0.94	0.93	0.96	0.99	--	0.96	1.01
200×75-t4.0-N100-A0.4-FR	93.45	0.82	0.86	0.99	0.86	0.84	--	0.87	0.86	0.83	1.00	0.98	--	0.94	1.01
250×100-t6.0-N50-A0.2-FR	152.61	0.99	0.99	0.99	1.01	0.92	--	0.96	0.95	1.00	0.98	1.08	--	1.03	1.04
250×100-t6.0-N50-A0.4-FR	152.61	0.92	0.98	0.98	0.88	0.82	--	0.86	0.87	0.94	1.11	1.12	--	1.07	1.13
250×100-t4.0-N100-A0.2-FR	100.81	0.94	0.98	0.99	0.99	0.93	--	0.96	0.94	0.95	0.99	1.01	--	0.97	1.04
250×100-t4.0-N100-A0.4-FR	100.81	0.81	0.88	0.99	0.87	0.83	--	0.87	0.86	0.82	1.01	0.98	--	0.93	1.03
Average										0.92	1.00	1.03		0.98	1.03
Cov										0.06	0.05	0.04		0.04	0.05
Lipped sections with ferritic stainless steel															
110×74×33-t1.5-N50-A0.2-FR	6.49	0.90	0.95	1.00	0.99	0.94	--	0.97	0.94	0.91	0.96	0.96	--	0.93	1.00
110×74×33-t1.5-N75-A0.2-FR	6.82	0.93	0.94	1.00	0.97	0.95	--	0.98	0.94	0.93	0.96	0.98	--	0.95	1.00
110×74×33-t1.5-N100-A0.2-FR	7.16	0.95	0.94	--	0.96	0.97	--	0.98	0.93	--	--	0.98	--	0.96	1.01
200×74×33-t1.5-N50-A0.4-FR	5.18	0.76	0.85	0.98	0.88	0.82	--	0.87	0.86	0.78	0.96	0.93	--	0.88	0.99
200×74×33-t1.5-N75-A0.4-FR	5.33	0.78	0.84	0.99	0.87	0.83	--	0.87	0.85	0.79	0.97	0.94	--	0.90	0.99
200×74×33-t1.5-N100-A0.4-FR	5.48	0.80	0.85	0.99	0.86	0.84	--	0.87	0.85	0.81	0.98	0.96	--	0.92	1.00
Average										0.84	0.97	0.96	--	0.92	1.00
Cov										0.06	0.01	0.02	--	0.03	0.01
Lipped sections with duplex stainless steel															
110×74×33-t1.5-N50-A0.2-FR	6.49	0.92	0.95	1.00	0.99	0.94	--	0.97	0.94	0.92	0.96	0.98	--	0.95	1.00
110×74×33-t1.5-N75-A0.2-FR	6.82	0.93	0.95	1.00	0.97	0.95	--	0.98	0.94	0.93	0.98	0.98	--	0.95	1.02
110×74×33-t1.5-N100-A0.2-FR	7.16	0.94	0.96	--	0.96	0.97	--	0.98	0.93	--	1.00	0.97	--	0.95	1.03
200×74×33-t1.5-N50-A0.4-FR	5.18	0.81	0.85	0.98	0.88	0.82	--	0.87	0.86	0.83	0.97	0.99	--	0.94	0.99
200×74×33-t1.5-N75-A0.4-FR	5.33	0.82	0.86	0.99	0.87	0.83	--	0.87	0.85	0.84	0.98	0.99	--	0.95	1.00
200×74×33-t1.5-N100-A0.4-FR	5.48	0.83	0.86	0.99	0.86	0.84	--	0.87	0.85	0.84	1.00	1.00	--	0.96	1.01
Average										0.87	0.98	0.98	--	0.95	1.01

Cov										0.04	0.02	0.01	--	0.01	0.01
Lipped sections with austenitic stainless steel															
110×74×33-t1.5-N50-A0.2-FR	6.49	0.91	0.95	1.00	0.99	0.94	--	0.97	0.94	0.91	0.96	0.97	--	0.94	1.00
110×74×33-t1.5-N75-A0.2-FR	6.82	0.93	0.94	1.00	0.97	0.95	--	0.98	0.94	0.93	0.97	0.98	--	0.95	1.01
110×74×33-t1.5-N100-A0.2-FR	7.16	0.94	0.95	--	0.96	0.97	--	0.98	0.93	--	0.99	0.98	--	0.96	1.02
200×74×33-t1.5-N50-A0.4-FR	5.18	0.77	0.85	0.98	0.88	0.82	--	0.87	0.86	0.78	0.97	0.93	--	0.89	0.99
200×74×33-t1.5-N75-A0.4-FR	5.33	0.78	0.85	0.99	0.87	0.83	--	0.87	0.85	0.80	0.97	0.95	--	0.90	0.99
200×74×33-t1.5-N100-A0.4-FR	5.48	0.81	0.85	0.99	0.86	0.84	--	0.87	0.85	0.82	0.99	0.96	--	0.92	1.00
Average										0.85	0.97	0.96	--	0.93	1.00
Cov										0.06	0.01	0.02	--	0.03	0.01

7.2 Reliability of proposed equations

Using the approach described by Hsiao et al. [45], a detailed reliability analysis was undertaken to assess the prediction performance of the proposed design equations. According to AS/NZS 4673:2001 [6], any design equation is deemed trustworthy if the reliability index (β') is greater than or equal to the desired reliability index of 2.50. The values determined by the proposed equations are greater than the target index for unfastened and fastened cold-formed stainless steel channels, as shown in Tables 11 and 12. This demonstrates that the equations (26-29) are as reliable as FEA results when used to determine the ITF web crippling strength of cold-formed stainless steel perforated channels.

Table 11 Reliability analysis summary for proposed equations on web crippling strength

(a) Unfastened sections

	Ferritic stainless steel		Duplex stainless steel		Austenitic stainless steel	
Ratio of equations	P_{DBN}/P_{prop}	P_{FEA}/P_{prop}	P_{DBN}/P_{prop}	P_{FEA}/P_{prop}	P_{DBN}/P_{prop}	P_{FEA}/P_{prop}
Mean, P_m	1.03	1.02	1.05	1.03	1.06	1.02
β	3.05	3.11	3.15	3.16	3.15	3.16
φ	0.7		0.7		0.7	

(b) Fastened sections

	Ferritic stainless steel		Duplex stainless steel		Austenitic stainless steel	
Ratio of equations	P_{DBN}/P_{prop}	P_{FEA}/P_{prop}	P_{DBN}/P_{prop}	P_{FEA}/P_{prop}	P_{DBN}/P_{prop}	P_{FEA}/P_{prop}
Mean, P_m	1.00	1.00	1.04	1.04	1.01	1.00
β	3.15	3.16	3.28	3.30	3.25	3.25
φ	0.70		0.70		0.70	

Table 12 Reliability analysis summary for proposed equations on web crippling strength reduction factor

(a) Unfastened sections with centred web hole using DBN prediction results

	Ferritic stainless steel		Duplex stainless steel		Austenitic stainless steel	
Ratio of equations	R_{DBN}/R_{prop}	R_{FEA}/R_{prop}	R_{DBN}/R_{prop}	R_{FEA}/R_{prop}	R_{DBN}/R_{prop}	R_{FEA}/R_{prop}
Mean, P_m	1.00	1.00	1.00	1.00	1.00	1.00
β	3.41	3.43	3.48	3.50	3.48	3.50
φ	0.70		0.70		0.70	

(b) Unfastened sections with offset web hole using DBN prediction results

	Ferritic stainless steel		Duplex stainless steel		Austenitic stainless steel	
Ratio of equations	R_{DBN}/R_{prop}	R_{FEA}/R_{prop}	R_{DBN}/R_{prop}	R_{FEA}/R_{prop}	R_{DBN}/R_{prop}	R_{FEA}/R_{prop}
Mean, P_m	1.00	1.00	1.00	1.00	1.00	1.00
β	3.47	3.48	3.48	3.48	3.47	3.50
φ	0.70		0.70		0.70	

(c) Fastened sections with centred web hole using DBN prediction results

	Ferritic stainless steel		Duplex stainless steel		Austenitic stainless steel	
Ratio of equations	R_{DBN}/R_{prop}	R_{FEA}/R_{prop}	R_{DBN}/R_{prop}	R_{FEA}/R_{prop}	R_{DBN}/R_{prop}	R_{FEA}/R_{prop}
Mean, P_m	1.00	1.00	1.00	1.00	1.00	1.00
β	3.48	3.50	3.48	3.48	3.52	3.55
φ	0.70		0.70		0.70	

(d) Fastened sections with offset web hole using DBN prediction results

	Ferritic stainless steel		Duplex stainless steel		Austenitic stainless steel	
Ratio of equations	R_{DBN}/R_{prop}	R_{FEA}/R_{prop}	R_{DBN}/R_{prop}	R_{FEA}/R_{prop}	R_{DBN}/R_{prop}	R_{FEA}/R_{prop}
Mean, P_m	1.00	1.00	1.00	1.00	1.00	1.00
β	3.53	3.52	3.47	3.48	3.51	3.51
φ	0.70		0.70		0.70	

390

8 Conclusions and future studies

The ITF web crippling structural behavior of cold-formed stainless steel perforated channels was investigated using a developed DBN model. Three common stainless steel grades were used: S43000 ferritic, S32205 duplex, and S30400 austenitic. The developed DBN model was trained with 43,200 data points created using the validated FE modeling techniques. From comparison with 54 experimental data taken from published literature, the DBN predictions are 7% conservative for unfastened sections and 11% conservative for fastened sections.

The accuracy of several approaches, such as DBN, BPN, Paddle model, and current standards, was assessed by comparing the error to the available test data. The developed DBN's accuracy was also compared to that of traditional prediction models (BPN and Paddle model) and outperformed the traditional models for certain training data, with average Err of 6.8% and 4.9% against experimental results for unfastened sections and fastened sections, respectively. Similarly, the developed DBN's accuracy was verified by comparing its results to calculated design strengths. The ASCE 8-02, EC3, and AISI&AS/NZS design strengths were over-conservative by 9.8%, 14.0 %, and 15.0 % for unfastened sections, respectively, and by 36.5 %, 43.7 %, and 3.9 % for fastened sections, respectively.

Based on the DBN results, new design equations were developed in order to determine the ITF web crippling strengths in terms of using strength reduction factors for cold-formed stainless steel (ferritic, duplex, and austenitic) channels. The feasibility of the proposed design equations was then checked by using a reliability analysis, and it was found that the proposed equations are reliable to determine the ITF web crippling strength of cold-formed

stainless steel perforated channels.

Some limitations were summarized in this study. The real effect of geometric imperfection and residual stresses on the web crippling behavior of cold-formed stainless steel channels is unclear. The current material model of stainless steel used in this paper should be improved to match the failure process of cold-formed stainless steel channels subjected to ITF web crippling loading. In this paper, the proposed equations cover the typical ITF web crippling case, however, in engineering practice, the loading condition and boundary condition may vary.

The aforementioned limitations indicate the need for further research in the following areas:

- The effects of geometric imperfection and residual stresses on the way thin-walled structural members behave should be studied using both experiments and computer simulations.
- The different material models of stainless steel should be checked for the web crippling case.
- Modifications to the web crippling coefficients of design standards should be made for sections with complicated loads and boundary conditions.

References

[1] A. McIntosh, P. Gatheeshgar, S. Gunalan, E. Kanthasamy, K. Poologanathan, M. Corradi, C. Higgins, Unified approach for the web crippling design of cold-formed channels: Carbon steel, stainless steel and aluminium. J. Build. Eng. 51 (2022) 104134.

[2] A. McIntosh, P. Gatheeshgar, K. Poologanathan, S. Gunalan, S. Navaratnam, C. Higgins, Web crippling of cold-formed carbon steel, stainless steel, and aluminium channels: Investigation and design. J. Constr. Steel Res. 179 (2021) 106538.

[3] X. Chen, H. Yuan, X. Du, Y. Zhao, J. Ye, L. Yang, Shear buckling behaviour of welded stainless steel plate girders with transverse stiffeners. Thin-Walled Struct. 122 (2018) 529–544.

[4] H. T. Li, B. Young, Web crippling of cold-formed ferritic stainless steel square and rectangular hollow sections. Eng. Struct. 176 (2018) 968–980.

[5] American Society of Civil Engineers (ASCE), Specification for the Design of Cold-formed Stainless Steel Structural Members, SEI/ASCE 8-02, Reston, Va, 2002.

[6] Australian/New Zealand Standard (AS/NZS), Cold-Formed Stainless Steel Structures, AS/NZS 4673:2001, Standards Australia, Sydney, Australia, 2001.

[7] Eurocode 3: Design of steel structures—Part 1.4 (EN 1993-1-4). General rules—Supplementary rules for stainless steels. European Committee for Standardization (CEN), Brussel; 2006.

[8] M. Bock, I. Arrayago, E. Real, E. Mirambell, Study of web crippling in ferritic stainless steel cold formed sections. Thin-Walled Struct. 69 (2013) 29–44.

[9] G. Santos, L. Gardner, Simplified and advanced design for stainless steel members under concentrated transverse loading. Ce/Papers, 4(2–4) (2021) 1513–1522. https://doi.org/10.1002/cepa.1450

[10] Z. Fang, K. Roy, Y. Chi, B. Chen, J. B. Lim, Finite element analysis and proposed design rules for cold-formed stainless steel channels with web holes under end-one-flange loading. Struct. 34 (2021) 2876–2899.

[11] Z. Fang, K. Roy, A. Uzzaman, J. B. Lim, Numerical simulation and proposed design rules of cold-formed stainless steel channels with web holes under interior-one-flange loading. Eng. Struct. 252 (2022) 113566.

[12] A. M. Yousefi, J. B. P. Lim, G. Charles Clifton, Cold-formed ferritic stainless steel unlipped channels with web openings subjected to web crippling under interior-two-flange loading condition – Part I: Tests and finite element model validation. Thin-Walled Struct. 116 (2017) 333–341.

[13] A. M. Yousefi, J. B. P. Lim, G. Charles Clifton, Cold-formed ferritic stainless steel unlipped channels with web openings subjected to web crippling under interior-two-flange loading condition – Part II: Parametric study and design equations. Thin-Walled Struct. 116 (2017) 342–356.

[14] A. M. Yousefi, B. Samali, I. Hajirasouliha, Y. Yu, G. C. Clifton, Unified design equations for web crippling failure of cold-formed ferritic stainless steel unlipped channel-sections with web holes. J. Build. Eng. 45 (2022) 103685.

[15] A. M. Yousefi, A. Uzzaman, J. B. P. Lim, G. C. Clifton, B. Young, Numerical investigation of web crippling strength in cold-formed stainless steel lipped channels with web openings subjected to interior-two-flange loading condition. Steel Compos Struct. 23 (3) (2017) 363–383.

[16] H. Liu, Y. Zhang, Image-driven structural steel damage condition assessment method using deep learning algorithm. Meas, 133 (2019) 168-181.

[17] R. Ali, Y.-J. Cha, Subsurface damage detection of a steel bridge using deep learning and uncooled micro-bolometer. Constr Build Mater. 226 (2019) 376-387.

[18] T. V. Hung, V. Q. Viet, D. V. Thuat, A deep learning-based procedure for estimation of ultimate load carrying of steel trusses using advanced analysis, J. Sci. Technol. Civ. Eng. 13 (3) (2019) 113-123.

[19] G. Papazafeiropoulos, QV. Vu, VH. Truong, MC. Luong, VT. Pham, Prediction of buckling coefficient of stiffened plate girders using deep learning algorithm. In: C. Ha-Minh, D. Dao, F. Benboudjema, S. Derrible, D. Huynh, A. Tang, (eds) CIGOS 2019, Innovation for Sustainable Infrastructure. Lecture Notes in Civil Engineering, vol 54 (2020). Springer, Singapore.

[20] Xu, Y., Zhang, M., & Zheng, B. Design of cold-formed stainless steel circular hollow section columns using machine learning methods. Structures, 33 (2021) 2755–2770.

[21] Z. Fang, K. Roy, J. Xu, Y. Dai, B. Paul, J. B.P. Lim, A novel machine learning method to investigate the web crippling behaviour of perforated roll-formed aluminium alloy unlipped channels under interior-two flange loading. Journal of Building Engineering, 51 (2022) 104261.

[22] Y. Dai, K. Roy, Z. Fang, B. Chen, G. M. Raftery, J. B.P. Lim, A novel machine learning model to predict the moment capacity of cold-formed steel channel beams with edge-stiffened and un-stiffened web holes. J. Build. Eng. 53 (2022) 104592.

[23] Z. Fang, K. Roy, Q. Ma, A. Uzzaman, J.B.P. Lim, Application of deep learning method in web crippling strength prediction of cold-formed stainless steel channel sections under end-two-flange loading, Struct. 33 (2021) 2903-2942.

[24] Z. Fang, K. Roy, B. Chen, C.-W. Sham, I. Hajirasouliha, J.B.P. Lim, Deep learning-based procedure for structural design of cold-formed steel channel sections with edge-stiffened and un-stiffened holes under axial compression, Thin-Walled Struct. 166 (2021) 108076.

[25] Z. Fang, K. Roy, J. Mares, C. W. Sham, B. Chen, J.B.P. Lim, Deep learning-based axial capacity prediction for cold-formed steel channel sections using Deep Belief Network. Struct. 33 (2021) 2792–2802.

[26] Z. Fang, K. Roy, J. M. Ingham, J.B.P. Lim, Assessment of end-two-flange web crippling strength of roll-formed aluminium alloy perforated channels by experimental testing, numerical simulation, and deep learning. Eng. Struct. 268 (2022) 114753.

[27] Z. Fang, K. Roy, Y. Dai,. J.B.P. Lim, Effect of web perforations on end-two-flange web crippling behaviour of roll-formed aluminium alloy unlipped channels through experimental test, numerical simulation and deep learning. Thin-Walled Struct. 179 (2022) 109489.

[28] B. Company, PaddlePaddle-based AI, [Online]. Available: http://en.paddlepaddle.org/.

[29] ABAQUS Analysis User's Manual-Version 6.14-2, ABAQUS Inc., USA, 2018.

[30] I. Arrayago, E. Real, L. Gardner, Description of stress–strain curves for stainless steel alloys. Mater. Des. 87 (2015) 540–552.

[31] E. Mirambell, E. Real, On the calculation of deflections in structural stainless steel beams: an experimental and numerical investigation, J. Constr. Steel Res. 54 (4) (2000) 109–133.

[32] K.J.R. Rasmussen, Full-range stress–strain curves for stainless steel alloys, J. Constr. Steel Res. 59 (1) (2003) 47–61.

[33] Dar, M. A., Sahoo, D. R., & Jain, A. K. (2019, November). Axial compression behavior of laced cold-formed steel built-up columns with unstiffened angle sections. Journal of Constructional Steel Research, 162, 105727. https://doi.org/10.1016/j.jcsr.2019.105727

[34] Zhang, X., Rasmussen, K. J., & Zhang, H. (2015, November). Structural modeling of cold-formed steel portal frames. Structures, 4, 58–68. https://doi.org/10.1016/j.istruc.2015.10.010

[35] A. Uzzaman, J.B.P. Lim, D. Nash, J. Rhodes, B. Young, Web crippling behaviour of cold-formed steel channel sections with offset web holes subjected to interior two flange loading, Thin-Walled Struct. 50 (2012) 76–86.

[36] A. Uzzaman, J.B.P. Lim, D. Nash, J. Rhodes, B. Young, Cold-formed steel sections with web openings subjected to web crippling under two-flange loading conditions—Part I: tests and finite element analysis, Thin-Walled Struct. 56 (2012) 38–48.

[37] A. Uzzaman, J.B.P. Lim, D. Nash, J. Rhodes, B. Young, Cold-formed steel sections with web openings subjected to web crippling under two-flange loading conditions—Part II: parametric study and proposed design equations, Thin-Walled Struct. 56 (2012) 79–87.

[38] American Iron and Steel Institute (AISI). North American Specification for the Design of Cold-formed Steel Structural Members AISI S100-16; 2016.

[39] Australia/New Zealand Standard (AS/NZS). Cold-Formed Steel Structures, AS/NZS 4600:2018. Standards Australia/ Standards New Zealand; 2018.

[40] Eurocode 3: Design of steel structures—Part 1.3 (EN 1993-1-3). General rules—Supplementary rules for cold-formed members and sheeting. European Committee for Standardization (CEN), Brussel; 2006.

[41] C. Li, Z. Ding, J. Yi, Y. Lv, G. Zhang, Deep belief network based hybrid model for building energy consumption prediction, Energies. 11 (1) (2018) 242.

[42] H.W. Ian, F. F. Eibe, A. H. Mark, J. P. Christopher, Data mining (Fourth Edition), New Zealand, 2017.

[43] B. Zhao, H. Xiong, J. Bian, Z. Guo, C. Xu, D. Dou, COMO: Widening deep neural networks with convolutional maxout. IEEE T. Multimed. (2020) 1-1.

[44] IBM Corp. (2020). IBM SPSS Statistics for Windows (Version 27.0). IBM Corp.

[45] L. Hsiao, W. Yu, T.V. Galambos, Load and resistance factor design of cold formed steel, calibration of the AISI design provisions, Ninth Progress Report, Civil Engineering Study 88-2, University of Missouri-Rolla, Rolla, Missouri, U.S.A., February 1988.

Notation

a	Hole diameter;
a/h	Hole diameter to web flat depth;
b_w	Overall web depth of section;
b_f	Overall flange width of section;
b_l	Lip flat width;
b_l/t	Ratio of lip to thickness;
c_1	Width of top lip;
c_2	Width of bottom lip;
C, C_1, C_2, C_θ, C_t	Coefficients from ASCE 8-02;
CFCS	Cold-formed carbon steel;
CFSS	Cold-formed stainless steel;
Cov	Coefficient of variation;
DBN	Deep Belief Network;
d	Overall web depth of section;
d_w	Web height between flange mid-lines;
d/b_f	Ratio of web to flange;
d/b_l	Ratio of web to lip;

e_0	Member imperfection magnitude;
E	Young's modulus;
Err	Absolute percentage error;
$E_{0.2}$	Tangent modulus at 0.2% of proof stress;
EOF	End-one-flange loading condition;
ETF	End-two-flange loading condition;
f_u	Ultimate material tensile strength;
f_y	Material yield stress;
$f_{0.2}$	0.2% of proof stress;
$f_{0.05}$	0.05% of proof stress;
FEA	Finite element analysis;
h	Depth of the flat portion of web;
h/t	Web flat depth to web thickness;
IOF	Interior-one-flange loading condition;
ITF	Interior-two-flange loading condition;
k_1,k_2,k_3,k_4,k_5	Coefficients from EC3;
k_L	Coefficient from the length control equation;
L	Length of channel section;
m, n	Strain hardening exponents;
MAE	Mean absolute error;
MSE	Mean squared error;
n_d	Number of data series;
n_h	Hole number;
N	Bearing length;
N/h	Bearing length to web flat depth;
N/t	Bearing length to web thickness;
P_{A0}	Web crippling strength of sections without holes;
$P_{\text{AISI\&AS/NZS}}$	Predicted web crippling strength of cold-formed stainless steel channel section from AISI S100-16 and AS/NZS 4600:2018;

P_{DBN}	Predicted web crippling strength of cold-formed stainless steel channel section from DBN;
P_{EXP}	Web crippling strength from experiments;
P_{FEA}	Web crippling strength from the finite element analysis;
P_c	Web crippling strength value from the training database;
P_p	Predicted web crippling strength value;
P_{prop}	Web crippling strength from proposed equations;
P_w	Web crippling strength with web holes from Yousefi et al.;
r	Inside bend radius;
r/t	Section inside bend radius to web thickness;
R	Web crippling strength reduction factor;
R^*	Correlation coefficient;
R_{DBN}	Reduction factor from DBN output;
R_{prop}	Reduction factor from proposed equations;
R_{Yousefi}	Reduction factor from Yousefi et al.;
t	Section/web thickness;
x	Hole distance to bearing block;
x/h	Hole distance to web flat depth;
X_i	Value of variables of input vectors;
$\overline{X}$	Mean value of variables of input vectors;
υ	Passion ratio;
$\upsilon_{\mathrm{elastic}}$	Poisson ratio at elastic stage;
$\upsilon_{\mathrm{plastic}}$	Poisson ratio at plastic stage
$\sigma_{0.05}$	0.05% proof stress;
ε_u	Ultimate strain;
$\alpha, \beta, \gamma, \lambda, \rho, \mu, \zeta, \zeta$	Equation coefficients;